

AN IMPROVEMENT OF DOA ESTIMATION ON RFID SYSTEMS

**M.Sc. Thesis by
Nida SAKAR**

Department : Electronics and Communication
Engineering
Telecommunication Engineering

JANUARY 2011

AN IMPROVEMENT OF DOA ESTIMATION ON RFID SYSTEMS

**M.Sc. Thesis by
Nida SAKAR
(504081325)**

**Date of submission : 20 December 2010
Date of defence examination: 17 January 2011**

**Supervisor (Chairman) : Assis. Prof. Dr. Mesut KARTAL (ITU)
Members of the Examining Committee : Prof. Dr. Sedef KENT (ITU)
Prof. Dr. Tülay YILDIRIM (YTU)**

JANUARY 2011

İSTANBUL TEKNİK ÜNİVERSİTESİ ★ FEN BİLİMLERİ ENSTİTÜSÜ

RFID SİSTEMLERİNDE DOA KESTİRİMİNİN İYİLEŞTİRİLMESİ

YÜKSEK LİSANS TEZİ
Nida SAKAR
(504081325)

Tezin Enstitüye Verildiği Tarih : 20 Aralık 2010

Tezin Savunulduğu Tarih : 17 Ocak 2011

Tez Danışmanı : Yar. Doç. Dr. Mesut KARTAL (İTÜ)
Diğer Jüri Üyeleri : Prof. Dr. Sedef KENT (İTÜ)
Prof. Dr. Tülay YILDIRIM (YTÜ)

OCAK 2011

To my uncle, Hasan KARAASLAN

FOREWORD

I would like to express my deep appreciation and thanks for my advisor, Mesut KARTAL who shared his time, experiences and suggestions with me during my bachelor and master education periods.

I also would like to thank Dr. Gregory HISLOP and Prof. Dr. Christophe CRAEYE from Telecommunication Department of Universite Catholique de Louvain for their support and encouragement.

Finally, I am very thankful to my family and my friends for their constant support and love. This work is supported by ITU Institute of Science and Technology and UCL Telecommunication Department.

December 2010

Nida SAKAR

Telecommunication Engineer

TABLE OF CONTENTS

	<u>Page</u>
TABLE OF CONTENTS	ix
ABBREVIATIONS	xi
LIST OF FIGURES	xiii
SUMMARY	xv
ÖZET	xvii
1. INTRODUCTION	1
2. DIRECTION OF ARRIVAL (DOA) ESTIMATION	3
2.1 Background on Array Processing.....	3
2.1.1 Data model.....	3
2.1.2 Eigen-structure of the spatial covariance matrix.....	5
2.1.3 Antenna beamforming.....	8
2.2 Direction of Arrival Estimation Techniques.....	8
2.2.1 Classical methods.....	8
2.2.1.1 Delay and sum method.....	8
2.2.1.2 Capon algorithm.....	9
2.2.2 Subspace methods.....	10
2.2.2.1 Multiple signal classification (MUSIC) algorithm.....	11
2.2.2.2 The root-MUSIC algorithm.....	12
2.2.2.3 The minimum norm method.....	13
2.2.2.4 Estimation of signal parameters via rotational invariance techniques (ESPIRIT)	15
2.2.3 The maximum likelihood techniques.....	18
2.3 Summary.....	19
3. 2D DIRECTION FINDING SYSTEM AND RECALIBRATION OF THE ARRAY	21
3.1 2D Direction Finding System.....	21
3.1.1 Uniform circular array.....	21
3.1.2 RF/BF circuits of the direction finding system.....	23
3.1.3 Digital signal processing (DSP)	24
3.2. Array Recalibration of the Direction Finding System.....	25
3.2.1 Array calibration.....	26
3.2.1.1 Remote transmitter approach.....	26
3.2.1.2 Test tone approach.....	27
3.2.2 Array recalibration.....	29
4. DOA ESTIMATION of PASSIVE RFID TAGS in MULTIPATH ENVIRONMENT	39
4.1 Spatial Smoothing	39
4.1.1 Problem statement.....	39
4.1.2 Spatial smoothing algorithm.....	41

4.2 The Interpolated Array Technique.....	44
4.3 Iterative Spatial Smoothing Algorithm for 2D Direction Finding.....	46
5. POST-PROCESSING APPROACH to MUSIC ALGORITHM for 2D	
DIRECTION FINDING SYSTEM: CLEAN ALGORITHM.....	53
5.1 Interferometry.....	53
5.2 Mathematical Link between Interferometry and MUSIC Algorithm.....	55
5.3 CLEAN Algorithm.....	57
5.4 Simulated Results.....	58
5.5 Measured Results.....	65
6. CONCLUSION	69
REFERENCES.....	71
APPENDICES.....	75
CURRICULUM VITAE.....	77

ABBREVIATIONS

ADC	: Analogue/Digital Converter
BA	: Baseband Amplifier
CM	: Clean Map
CB	: Clean Beam
DOA	: Direction of Arrival
DB	: Dirty Beam
DFT	: Discrete Fourier Transform
DM	: Dirty Map
DSP	: Digital Signal Processing
ESPIRIT	: Estimation of Signal Parameters via Rotational Invariance Techniques
FFT	: Fast Fourier Transform
I&Q	: In-phase & Quadrature
LNA	: Low Noise Amplifier
ML	: Maximum Likelihood
MVDR	: Minimum Variance Distortionless Response
MUSIC	: Multiple Signal Classification
RF/BF	: Radio Frequency/Baseband Frequency
SNR	: Signal-to-Noise Ratio
SVD	: Singular Value Decomposition
UCA	: Uniform Circular Array
ULA	: Uniform Linear Array

LIST OF FIGURES

	<u>Page</u>
Figure 2.1: Data Model geometry.....	4
Figure 2.2: DOA estimation of Delay and Sum Method and Capon Algorithm for ULA	10
Figure 2.3: Block diagram of MUSIC algorithm.....	12
Figure 2.4: An example for root-MUSIC array geometry.....	12
Figure 2.5: Antenna array structure of ESPRIT Algorithm for multiple source	15
Figure 2.6: The steps of ESPRIT Algorithm.....	18
Figure 3.1: Schematic diagram of 2D direction finding system.....	22
Figure 3.2: Uniform Circular Array with 8 slotted-box antennas.....	22
Figure 3.3: A slotted-box sensor.....	23
Figure 3.4: RF/BF Circuits' block diagram.....	23
Figure 3.5: A reader-tag communication example.....	24
Figure 3.6: Remote Transmitter Approach.....	27
Figure 3.7: The calibration position of the system.....	28
Figure 3.8: The contour plots of the estimated positions of a) the calibration tag b) the tag on the table and c) the tag above the calibration tag.....	30
Figure 3.9: The position of the dipole in front of the array.....	31
Figure 3.10: The contour plots of the estimated positions of a) the calibration tag b) the tag on the table and c) the tag above the calibration tag.....	33
Figure 3.11: The calibrating tag and the antenna array.....	34
Figure 3.12: Transmitting dipole and antenna array.....	35
Figure 3.13: The contour plots of the estimated positions of a) the calibration tag b) the tag on the table c) the tag above the calibration.....	38
Figure 4.1: Sub-array spatial smoothing.....	42
Figure 4.2: Block diagram of DOA estimation of coherent signals.....	44
Figure 4.3: Array shifting example for planar arrays such as UCAs.....	47
Figure 4.4: Results of the MUSIC algorithm for 3 correlated signals a) without spatial smoothing b) with spatial smoothing after 5 iterations.....	48
Figure 4.5: 2D direction finding system with coherent signals.....	49
Figure 4.6: Results of the MUSIC algorithm a) without metal plate b) with metal plate	50
Figure 4.7: The result of the MUSIC algorithm with suggested spatial smoothing algorithm.....	51
Figure 5.1: An interferometer with two antennas.....	54
Figure 5.2: Convolution schematic of intensity and dirty beam.....	55
Figure 5.3: Two uncorrelated sources located at $(x,y,z) = [-10,0,100]$ and $[10,0,100]$ (metres) a) MUSIC algo. result in the absence of noise b) MUSIC algo. result in the presence of noise c) CLEAN algo. result after three iterations in the presence of noise result after three iterations in noisy space.....	60
Figure 5.4: The final map of the power spectrum without adding residuals.....	61

Figure 5.5: Two uncorrelated sources a) MUSIC algo. result in noise free space b) CLEAN algo result in noise free space c) MUSIC algo. result in noisy space d) CLEAN algo. result after three iterations in noisy space.....	62
Figure 5.6: Three uncorrelated a) MUSIC algo. result in the absence of noise b) MUSIC algo. result in noisy space c) CLEAN algo. result after ten iterations in noisy space.....	63
Figure 5.7: Two uncorrelated a) MUSIC algo. result in noise free space b) CLEAN algo result in noise free space c) MUSIC algo. result in noisy space d) CLEAN algo.....	64
Figure 5.8: The measured results of MUSIC and CLEAN algorithms for two different amplitude and position conditions	66
Figure 5.9: The measured results of MUSIC and CLEAN algorithms for three sources.....	67

AN IMPROVEMENT OF DOA ESTIMATION IN RFID SYSTEMS

SUMMARY

Radio Frequency Identification (RFID) is a concept that identifies an object or a human being by using the electromagnetic wave coming from the target. RFID technology is used for security, access control and transportation, etc. Another application of RFID technology is estimating the direction of arrival of electromagnetic wave transmitter, for instance a passive RFID tag. The estimation of Direction of Arrival (DOA) is an important research field due to its application areas, for instance radar, sonar, radio astronomy, seismology, remote sensing, etc.

In this thesis, a set of studies related to 2-D direction finding system which is designed for localizing passive RFID tags is included. This system consists of antenna array, reader and data collector devices. Because of the tag's being passive, it uses the power of the incoming request signal which is transmitted by the dipole antenna connected to the reader to prepare a response and communicate with the system. This response is collected by the data collector device and sent to the personal computer. It is processed with Direction of Arrival estimation algorithm written in MATLAB and the localization of the tag in 2-D is found. The context of the thesis can be listed as follows: recalibration of the array cheaply and easily, localization of passive tags in multipath environment and proposition of applying a post-processing algorithm which is commonly used in radio astronomy imaging to the direction finding system.

RFID SİSTEMLERİNDE DOA KESTİRİMİNİN İYİLEŞTİRİLMESİ

ÖZET

Radio Frequency Identification (RFID); bir sistemin, kişinin veya objenin yaydığı elektromanyetik dalgayı kullanarak kimlik tanımasını açıklayan bir terimdir. RFID teknolojisi güvenlik, giriş kontrol ve taşımacılık gibi pek çok sektörde kullanılmaktadır. RFID teknolojisinin bir uygulaması da elektromanyetik dalga yayan kişi veya objenin yerinin tespit edilmesi çalışmalarıdır. Yer tespit etme çalışmalarının (Direction of Arrival Estimation) radar, sonar, radyoastronomi, sismoloji ve uzaktan algılama gibi pek çok önemli uygulama alanı olduğu için çok önemli bir araştırma alanıdır.

Bu tez çalışmasında, pasif RFID etiketlerinin 2-boyutta yerlerinin tespit edilmesi için geliştirilmiş sistemle yapılan çalışmalara yer verilmektedir. Bu sistem anten dizisi, okuyucu ve veri toplama cihazlarından oluşmaktadır. Sistem ve etiketin haberleşmesi, çalışmada kullanılan etiket pasif olduğundan okuyucuya bağlı bir dipol antenden yayılan işaretle gönderilen sorgu paketine, etiketin kendisine gelen dalgadan aldığı güçle cevap hazırlayıp göndermesi şeklinde olur. Cevap işareti anten dizisiyle alınıp veri toplama cihazından geçtikten sonra bilgisayara ulaşır. Bilgisayarda MATLAB program diliyle yazılmış algoritmaya işlenir ve etiketin yeri tespit edilir. Tez kapsamında yapılan çalışmalar anten dizisinin kolay ve ucuz bir şekilde tekrar kalibre edilmesi, yansız ortamda pasif etiketlerin doğru bir şekilde yerlerinin belirlenmesi ve son olarak radyoastronomik görüntülemeye kullanılan CLEAN algoritmasının yer tespit etme algoritmasında karşılaşılan bazı problemlerin çözümü olarak sunulması olarak sıralanabilir.

1. INTRODUCTION

Radio Frequency Identification (RFID) is a concept that identifying an object or a human being (target) by using the electromagnetic wave coming from the target. RFID is a widely used technology for security, access control, transportation, etc. Another application of RFID technology is estimating the direction of arrival of the electromagnetic wave transmitter, for instance an RFID tag.

Estimation of Direction of Arrival (DOA) is an important research field due to its application areas, such as radar, sonar, microphone sensors, radio astronomy, seismology, remote sensing and wireless communication systems [1-3]. In this work, the focus will be on 2-D direction finding system which is composed of transmitter, reader and a data collection device. The following questions will be answered in next chapters.

- Can this 2-D direction finding system be easily and cheaply recalibrated in the presence of noise outside of the laboratory?
- Does spatial smoothing technique work in multipath environment for this system?
- Can applying a post-processing algorithm –CLEAN- help to fix MUSIC Algorithm's problems?

This thesis will be organized as follows:

- Chapter 2 gives the basic review of Direction of Arrival estimation literature and introduces the data model which will be used throughout the thesis.
- Chapter 3 introduces 2-D direction finding system, calibration techniques for antenna arrays and proposes recalibration technique.
- Chapter 4 explains spatial smoothing technique for 2-D direction finding system in multipath environment, presents simulation and measured results for passive RFID tags.
- Chapter 5 presents mathematical link between MUSIC algorithm and interferometry and suggests using applying a post-processing method, called

CLEAN which is commonly used in interferometry imaging for radio astronomy, before the last step of the MUSIC algorithm.

- Finally, in Chapter 6, the conclusions will be drawn.

2. DIRECTION OF ARRIVAL (DOA) ESTIMATION

This chapter presents background on array processing and DOA estimation techniques. The data model, Eigen-structure of the spatial covariance matrix and antenna beamforming are the subheads of background on array processing. DOA estimation techniques can be classified as classical, subspace methods and Maximum Likelihood (ML). The classical DOA techniques: “Delay and Sum method” and “Capon algorithm” and the subspace techniques: “Multiple Signal Classification (MUSIC)”, “The Root-MUSIC Algorithm”, “The Minimum Norm Method” and “Estimation of Signal Parameters via Rotational Invariance Techniques (ESPRIT)” and Maximum Likelihood are briefly explained.

2.1 Background on Array Processing

The data model, the spatial covariance matrix, Eigen-structures of covariance matrix and antenna beam forming are the subjects of this section.

2.1.1 Data model

Assume that N array sensors receive r narrowband plane waves which have the same centre frequency (see Figure 2.1). The baseband signal, $s(t)$, reaches each element of the array at different time instants or phase delays (see Figure 2.1). Therefore, arrival time delay between the first and k th sensor comes out and the propagation delay Δt_k is [1]:

$$\Delta t_k = \frac{kD \sin \theta}{c} \quad (2.1)$$

where k is the wave number, θ is the angle between the sensor and plane wave, c is speed of light and D is distance between sensors [meter].

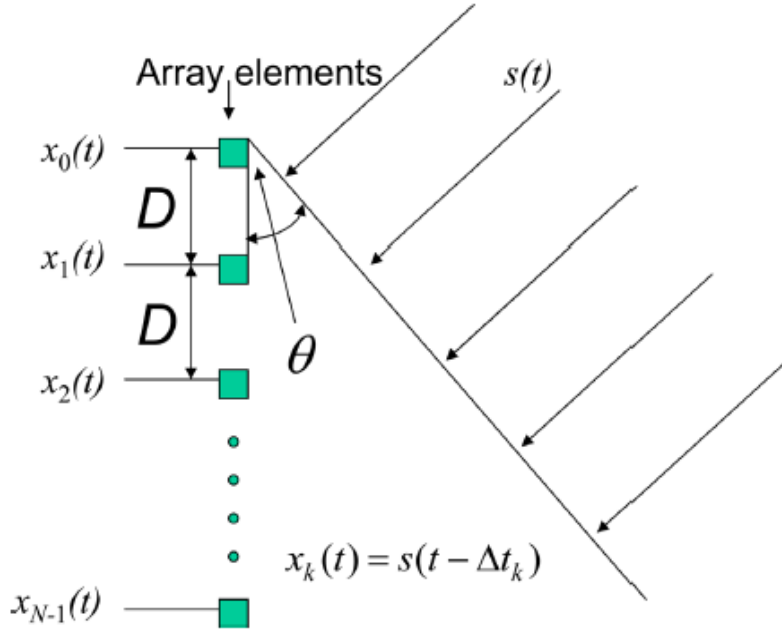


Figure 2.1: Data model geometry

The low-pass equivalent of the modulated signal $s_l(t)$ is down-converted to baseband. Received signal by the first sensor $s(t)$ and the baseband signal received by the k th sensor $x_k(t)$ are as follows [1]:

$$s(t) = \text{Re}\{s_l(t)e^{j2\pi f_c t}\} \quad (2.2)$$

$$x_k(t) = s_l(t - \Delta t_k)e^{-j2\pi f_c \Delta t_k} \quad (2.3)$$

where f_c is the centre frequency.

If the received signal is sampled with sampling period T (symbol period), it can be written as:

$$x_k(nT) = s_l(nT - \Delta t_k)e^{-j2\pi f_c \Delta t_k} \quad (2.4)$$

Each of the propagation delay across the array is much smaller than the sampling period $\Delta t_k \ll T$ in a wireless digital communication system; therefore the new form of the received signal is;

$$x_k(nT) = s_l(nT - \Delta t_k)e^{-j2\pi f_c \Delta t_k} \approx s_l(nT)e^{-j2\pi f_c \Delta t_k} \quad (2.5)$$

The distance between the elements of the array (D) should be equal or less than half wavelength [1]. Let us select $D = \lambda/2$ replace f_c with c/λ ,

$$x_k(nT) \approx s_i(nT)e^{-j\pi k \sin \theta} \quad (2.6)$$

The discrete time form of the signal can be expressed as [1]:

$$x_k[n] \approx s[n]e^{-j\pi k \sin \theta} = s[n]a_k(\theta) \quad (2.7)$$

In the presence of r signals which have the same centre frequency:

$$x_k[n] \approx \sum_{i=0}^{r-1} s_i[n]a_k(\theta_i) + v_k[n] \quad (2.8)$$

where $v_k[n]$ is additive noise at k th sensor.

By using matrix notation, the signal model of whole array can be written as [1]:

$$\begin{bmatrix} x_0[n] \\ x_1[n] \\ \vdots \\ x_{N-1}[n] \end{bmatrix} = \begin{bmatrix} a_0(\theta_0) & a_0(\theta_1) & \dots & a_0(\theta_{r-1}) \\ a_1(\theta_0) & \dots & \dots & a_1(\theta_{r-1}) \\ \vdots & \vdots & \vdots & \vdots \\ a_{N-1}(\theta_0) & a_{N-1}(\theta_1) & \dots & a_{N-1}(\theta_{r-1}) \end{bmatrix} \begin{bmatrix} s_0[n] \\ s_1[n] \\ \vdots \\ s_{r-1}[n] \end{bmatrix} + \begin{bmatrix} v_0[n] \\ v_1[n] \\ \vdots \\ v_{N-1}[n] \end{bmatrix} \quad (2.9)$$

The compact matrix form of the Eq. (2.9) is as follows:

$$x_n = [a(\theta_0) \ a(\theta_1) \ \dots \ a(\theta_{r-1})] s_n + v_n = A s_n + v_n \quad (2.10)$$

The $N \times 1$ column vector of the matrix A ($a(\theta_i)$) is defined as array response or steering vector of the signal $s_i(t)$ coming from direction θ_i . There is a direct relationship between DOA estimation and steering vector. In case of known steering vector for all directions, direction of arrivals can be estimated.

2.1.2 Eigen-structure of the spatial covariance matrix

To understand subspace method techniques, the Eigen-structure of the spatial covariance matrix of the data model should be known. The $N \times N$ spatial covariance matrix of received data whose signal and noise vectors assumed to be uncorrelated is [1]:

$$\begin{aligned} R_{xx} &= E[x_n x_n^H] = E[(A s_n + v_n)(A s_n + v_n)^H] = A E[s_n s_n^H] A^H + E[v_n v_n^H] \\ &= A R_{ss} A^H + \sigma^2 I_{N \times N} \end{aligned} \quad (2.11)$$

where v_n : Gaussian, zero mean white noise and its correlation matrix equals to $\sigma^2 I$.

Note that $R_{ss} = E[s_n s_n^H]$

This correlation matrix consists of two Eigen-spaces, signal subspace and noise subspace. These two subspaces are orthogonal to each other.

N dimensional subspace has r signal subspaces correspond to r incoming signals and N-r noise subspaces. The noise subspace is spanned by N-r linear independent eigenvectors (any of them= q_n). Each of the eigenvectors of the noise subspace is orthogonal to the columns of the matrix A.

$$R_{xx} q_n = (AR_{ss}A^H + \sigma^2 I)q_n = 0 + \sigma^2 Iq_n = \sigma^2 q_n \quad (2.12)$$

The Eigen-values of the corresponding Eigen-vectors of the noise subspace (q_i where $i=1, \dots, N-r$) are all equal to σ^2 . The signal subspace is spanned by r linear independent Eigen-vectors (any of them= q_s). Each of the Eigen-vectors of the signal subspace is also the Eigen-vector of the signal correlation matrix ($AR_{ss}A$).

$$R_{xx} q_s = (AR_{ss}A^H + \sigma^2 I)q_s = \sigma_s^2 q_s + \sigma^2 Iq_s = (\sigma_s^2 + \sigma^2)q_s \quad (2.13)$$

The Eigen-value of the corresponding Eigen-vectors of the signal subspace (q_i where $i=1, \dots, r$) is equal to $(\sigma_s^2 + \sigma^2)$, where σ_s^2 is the Eigen-value of $AR_{ss}A^H$.

The Eigen-decomposition of the correlation matrix is as follows with Q_s whose columns consist of r eigenvectors of signal subspace, Q_n whose columns consist of N-r eigenvectors of noise subspace, D_s which is a rxr diagonal matrix consists of r Eigen-values of signal eigenvectors and $\sigma^2 I$ which is a (N-r)x(N-r) diagonal matrix consists of (N-r) Eigen-values of noise eigenvectors [1,2].

$$\begin{aligned}
R_{xx} &= QDQ^H = [Q_s Q_n] \begin{bmatrix} D_s & 0 \\ 0 & \sigma^2 I \end{bmatrix} [Q_s Q_n]^H \\
&= Q \begin{pmatrix} \lambda_1 + \sigma^2 & 0 & \dots & 0 & 0 & \dots & 0 \\ 0 & \lambda_2 + \sigma^2 & \dots & 0 & 0 & \dots & 0 \\ \vdots & \vdots & \ddots & \vdots & \vdots & \vdots & \vdots \\ 0 & 0 & \dots & \lambda_r + \sigma^2 & 0 & \dots & 0 \\ 0 & 0 & \dots & 0 & \sigma^2 & \dots & 0 \\ \vdots & \vdots & \vdots & \vdots & \vdots & \ddots & \vdots \\ 0 & 0 & 0 & 0 & 0 & \dots & \sigma^2 \end{pmatrix} Q^H
\end{aligned} \tag{2.14}$$

There is another method to find Eigen-vectors of covariance matrix called Singular Value Decomposition (SVD). This method uses data matrix X whose rows consist of Hermitian transpose of the data vectors obtained from the antenna array. The basic assumptions are that X is formed by taking K snapshots; the array is linear and has N sensors. According to SVD, the KxN data matrix can be expressed as product of U, D and V matrices [1].

$$X = UDV^H \tag{2.15}$$

where U : KxK matrix, its columns are orthonormal, D : KxN diagonal matrix and V: NxN matrix, its columns are orthonormal, too.

There is a direct relationship between the Eigen-structures of covariance matrix of the data and data matrix. The columns of the V matrix are equal to Eigen-vectors and diagonal elements of D are equal to square roots of the Eigen-values. In practical situation, the covariance matrix is not known exactly and N-r smallest Eigen-values are not equal to σ^2 , but N-r smallest ones denote to noise Eigen-values. The value of the spatial covariance matrix should be estimated by using an estimator and the common estimator is as follows:

$$R_{xx} = \frac{1}{K} \sum_{i=0}^{K-1} x_n x_n^H \tag{2.16}$$

where K is the number of snapshots and x_n :is the received signal obtained by each sensor.

2.1.3 Antenna beamforming

Antenna beamforming is directly related to DOA estimation techniques. The antenna array is steered in a direction θ_1 at time t_1 and the output power is measured by beamforming techniques. In case of the steering angle's being DOA of a source, a significant peak occurs in the power spectrum. The array can be steered electronically by the knowledge of the array steering vector, but there might be a problem if the shape of the array pattern changes. To overcome this problem and form a single output signal, a weight vector which combines the data received by the sensors and is denoted by w can be designed. The output signal is [3]:

$$y(t) = w^H x(t) \quad (2.17)$$

The total averaged output power is [3]:

$$\begin{aligned} P(w) &= \frac{1}{N} \sum_{n=1}^N |y(t)|^2 = \frac{1}{N} \sum_{n=1}^N w^H x(t_n) x^H(t_n) w \\ &= w^H \hat{R}_{xx} w \end{aligned} \quad (2.18)$$

where N is the number of snapshots.

There are two well-known beamformer techniques called Conventional and Capon's Beamformer.

2.2 Direction of Arrival Estimation Techniques

2.2.1 Classical methods

The basic idea of classical DOA estimation methods is to steer the array on a particular angle and measure the output power of the system. Delay and Sum method and Capon algorithm are presented, respectively [1].

2.2.1.1 Delay and sum method

The Delay-and-Sum method is one of the classical DOA methods. The resolution that this algorithm provides can be improved by increasing the number of array sensors and this option is not desired because of the cost [1].

The Delay-and-Sum method finds the angle of arrival by choosing largest peaks in the power spectrum which is computed by measuring the signal power at each

possible angle of arrival. To evaluate a steering vector, the power coming from a certain direction is measured by generating a beam in that direction and the steering vector for corresponding direction equates to the beamformer weights. The output power of the beamformer of Delay and Sum method can be expressed as [1]:

$$P(\theta) = E[y^H y] = E|w^H x_n|^2 = E|a(\theta)^H x_n|^2 = a(\theta)^H R_{xx} a(\theta) \quad (2.19)$$

If w is equal to the steering vector of the incident signal ($w = a(\theta)$), the peaks come off in the power spectrum and the angle of arrival is found.

2.2.1.2 Capon algorithm

The other name of the Capon algorithm is Minimum Variance Distortionless Response (MVDR) algorithm. This algorithm is like Delay and Sum method which measures the signal power at each possible angle of arrival. The goal of this algorithm is to minimize the output power except the one that point the desired signal direction with respect to w for each possible angle of arrival while constraining the beamformer gain to be 1 to find the real direction of arrival value θ [1, 4].

$$\min_w E[|y(k)|^2] = \min_w w^H R w \quad \text{subject to } w^H a(\theta) = 1 \quad (2.20)$$

The peaks in the power spectrum in Eq. (2.20) are the estimated angles of arrival. Solving the above equation by the method of Lagrange Multipliers, its weights are found to be:

$$w = \frac{R^{-1} a(\theta)}{a(\theta)^H R^{-1} a(\theta)} \quad (2.21)$$

The Capon algorithm provides better resolution than Delay and Sum method and a simulation of the algorithms is presented below as a comparative example. In Figure 2.2, Uniform Linear Array (ULA) with 10 sensors (spacing $D = \lambda/2$) is used and all of the three sources have the same power level. It is clear that Capon Algorithm performs better resolution.

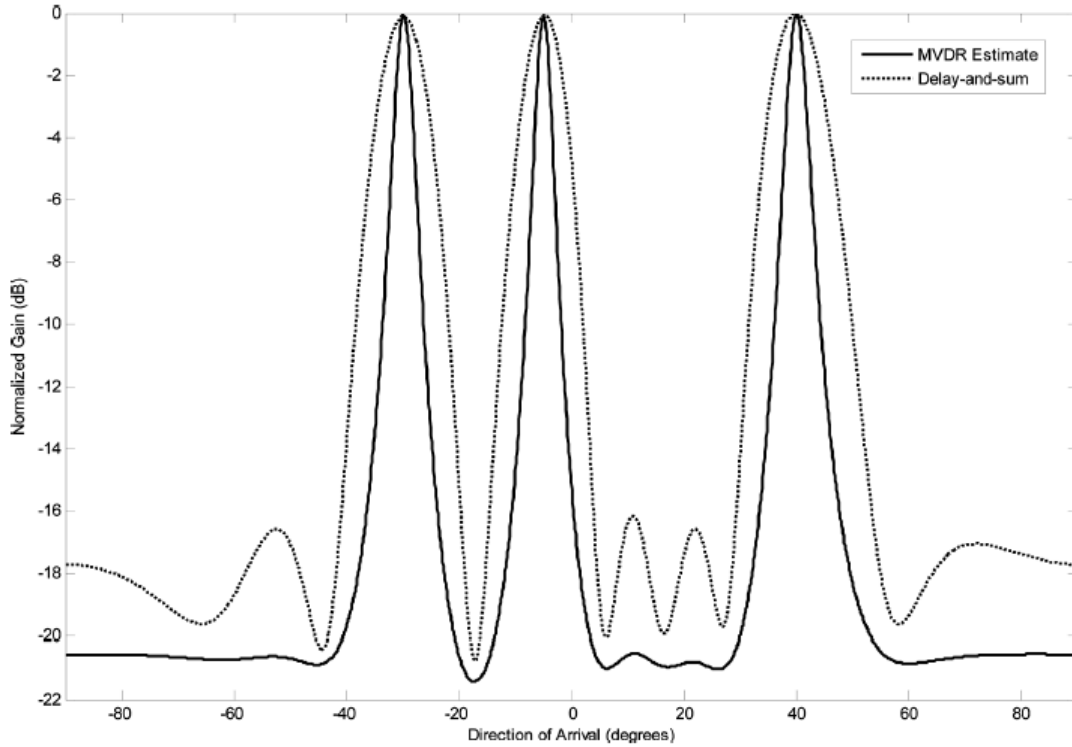


Figure 2.2: DOA estimation of Delay and Sum Method and Capon Algorithm for ULA [1].

2.2.2 Subspace methods

The subspace method uses its proven properties below [3]:

- 1) The spatial covariance matrix is spanned by its eigenvectors and the eigenvectors consist of two subspaces, which are both orthogonal, called signal and noise subspaces.
- 2) The steering vectors of the signal subspace
- 3) The eigenvectors regarding the smallest Eigen-values of the spatial covariance matrix span the noise subspace.
- 4) The eigenvectors regarding the largest Eigen-values of the spatial covariance matrix span the signal subspace.

Multiple Signal Classification (MUSIC), “The Root-MUSIC Algorithm”, “The Minimum Norm Method” and “Estimation of Signal Parameters via Rotational Invariance Techniques (ESPRIT)” are explained, respectively.

2.2.2.1 Multiple signal classification (MUSIC) algorithm

The Multiple Signal Classification Algorithm (MUSIC) is proposed by Schmidt in 1986 and it uses the feature which the steering vectors of the point sources are included in signal subspace and orthogonal to noise subspace. Point sources can be estimated by searching through all possible array steering vectors and pick the ones orthogonal to the noise subspace [1]. The steps of the MUSIC algorithm which is shown in Figure 2.3 can be summarized as follows [5-7]:

- 1) Compute the correlation matrix from the raw data
- 2) Perform an Eigen-decomposition of the correlation matrix. The eigenvectors corresponding to the largest r Eigen-values form the signal subspace and the rest ($N-r$) corresponds to the noise subspace.
- 3) Compute the power spectrum

Due to the steering vectors of the desired signal's being orthogonal to the noise subspace eigenvectors, $a^H(\theta)Q_nQ_n^H a(\theta) = 0$ for $\theta = \theta_i$. Therefore the power spectrum can be computed by taking the inverse of $a^H(\theta)Q_nQ_n^H a(\theta)$.

$$P(\theta) = \frac{1}{a^H(\theta)Q_nQ_n^H a(\theta)} \quad (2.22)$$

where $a(\theta)$ is the array response vector and it can be expressed as [5]:

$$a(\theta_k) = \begin{bmatrix} e^{j2\pi(r/\lambda)\cos(\theta_k)} \\ e^{j2\pi(r/\lambda)\cos\left(\theta_k - \frac{1}{N}2\pi\right)} \\ \vdots \\ e^{j2\pi(r/\lambda)\cos\left(\theta_k - \frac{N-1}{N}2\pi\right)} \end{bmatrix} \quad (2.23)$$

- 4) Find the location of the D largest peaks in the power spectrum

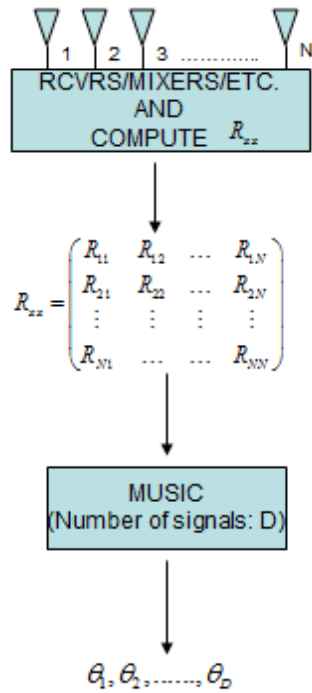


Figure 2.3: Block diagram of MUSIC algorithm.

Despite its great performance, MUSIC algorithm can't estimate the location of the signal in multipath environment. To defeat this disadvantage of MUSIC algorithm, the Spatial Smoothing technique might be used. This technique and this type of signals will be presented in the fourth chapter.

2.2.2.2 The root-MUSIC algorithm

The root MUSIC algorithm can be applied only to Uniform Linear Arrays (ULAs) and uniform array whose grid is regular as in Figure 2.4. This algorithm's resolution is better than the spectral search based MUSIC algorithm in the presence of low signal-to-noise ratios (SNRs).

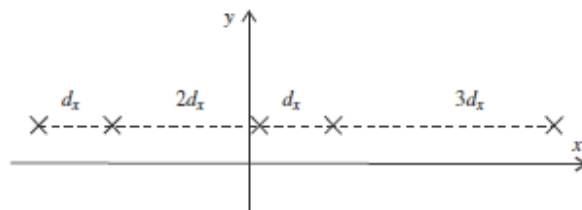


Figure 2.4: An example for root-MUSIC array geometry [8].

Assume that the array is ULA and its grid is on x-axis. The steering vector is as follows [8]:

$$a(\theta) = \begin{bmatrix} \exp\left\{-j\frac{N-1}{2}\frac{2\pi}{\lambda}D_x \sin\theta\right\} \\ \exp\left\{-j\frac{N-3}{2}\frac{2\pi}{\lambda}D_x \sin\theta\right\} \\ \vdots \\ \exp\left\{j\frac{N-1}{2}\frac{2\pi}{\lambda}D_x \sin\theta\right\} \end{bmatrix} = \begin{bmatrix} z^{-(N-1)/2} \\ z^{-(N-3)/2} \\ \vdots \\ z^{(N-1)/2} \end{bmatrix} \triangleq a(z) \quad (2.24)$$

where N is sensor number of ULA, D_x is the distance between sensors and $z \triangleq \exp\{j(2\pi/\lambda)D_x \sin\theta\}$

The root-MUSIC null-spectrum function can be expressed as follows by using Eq. (2.24) [8]:

$$f(\theta) = a^H(\theta)Q_N Q_N^H a(\theta) = a^T(1/z)Q_N Q_N^H a(z) \triangleq f(z) \quad (2.25)$$

The polynomial above has totally $2(N-1)$ roots consists of $(N-1)$ roots (z_i) and $(N-1)$ reciprocal roots ($1/z_i^*$) where * implies complex conjugate. In the absence of noise, r signal root pairs (root and its reciprocal) lying on the unit circle correspond to the signal roots and the rest sources $2(N-r-1)$ correspond to noise sources. In the presence of noise, the signal roots move a little through inside the unit circle and the closest r roots to the circle are estimated as signal roots.

2.2.2.3 The minimum norm method

Kumaresan and Tufts proposed the Minimum Norm Method and this method can be presented as improved version of MUSIC algorithm [1]. It is applicable for linear arrays and uses an arbitrary vector “ w ” called weight vector which lies on the noise subspace [1, 9].

$$a^H(\theta)w = 0 \quad (2.26)$$

$$w = \begin{bmatrix} 1 \\ \bar{w} \end{bmatrix} \quad (2.27)$$

The basic principal of this method is searching peaks in the power spectrum like MUSIC algorithm. The power spectrum is as follows [1, 9]:

$$P_{MN}(\theta) = \frac{1}{|a^H(\theta)W|^2} = \frac{1}{|a^H(\theta)Q_N Q_N^H W Q_N Q_N^H a(\theta)|} \quad (2.28)$$

where $a(\theta)$: steering vector and $W = p_1 p_1^T$ (p_1 : the first column of an $N \times N$ identity matrix)

If the expression of noise subspace is rewritten [9],

$$Q_N = [q_K, \dots, q_{N-1}] = \begin{bmatrix} q_{1,K}, \dots, q_{1,N-1} \\ q_{2,K}, \dots, q_{2,N-1} \\ \vdots \\ q_{N,K}, \dots, q_{N,N-1} \end{bmatrix} = \begin{bmatrix} h \\ H \end{bmatrix} \quad (2.29)$$

$$\text{where } h \triangleq [q_{1,K}, \dots, q_{1,N-1}] \quad \text{and} \quad H \triangleq \begin{bmatrix} q_{2,K}, \dots, q_{2,N-1} \\ \vdots \\ q_{N,K}, \dots, q_{N,N-1} \end{bmatrix}$$

A new noise subspace's first element should be one for letting the new vector's norm minimum and the new noise subspace consists of linear combination of the MUSIC noise subspace, hence it is still orthogonal to signal subspace [9].

$$Q'_N = H \cdot h^T \cdot (h \cdot h^T)^{-1} \quad (2.30)$$

$$Q_{NN} = \begin{bmatrix} 1 \\ Q'_N \end{bmatrix} \quad (2.31)$$

The new form of the power spectrum can be written as follows [9]:

$$P_{MN}(\theta) = \frac{1}{a^H(\theta)Q_{NN}Q_{NN}^H a(\theta)} \quad (2.32)$$

2.2.2.4 Estimation of signal parameters via rotational invariance techniques (ESPIRIT)

Most of the DOA estimation algorithms require the array steering matrix knowledge. The ways of obtaining array steering matrix are calibration in the field or calculating by using position and response information of each sensor of the array. This requirement is time-consuming and accuracy degrading because of the possible errors in calibration [3]. Since the Estimation of Signal Parameters via Rotational Invariance Technique (ESPIRIT) estimates the DOA by exploiting the rotational invariance of the signal subspaces of subsets of the array, it defeats these problems.

ESPIRIT constraints the array having two identical sub-array and each sub-array contains n sensors while total number of sensors in the array is N . An antenna pair consisting of a sensor in the first sub-array and its identical in the second sub-array is called doublet [10-12]. The distance between every matched pairs must be identical and the magnitude of the displacement in wavelengths is indicated by Δ . In Figure 2.5, antenna array structure of ESPIRIT for multiple sources can be seen. The total number of sensors in an array can be less than the total number of sensors in both sub-array ($N \leq 2n$), in other words one sensor can take place into both sub-array by overlapping. As long as sensors of every doublets have identical sensitivity patterns, the individual sensors of both sub-array can have arbitrary polarization, directional gain and phase response.

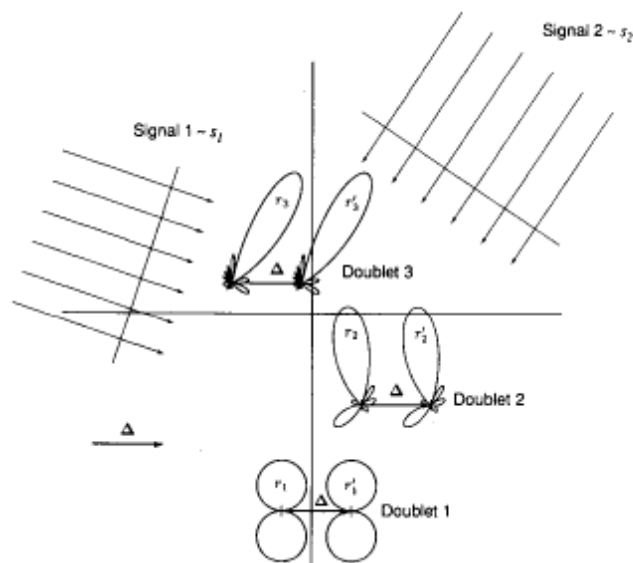


Figure 2.5: Antenna array structure of ESPIRIT Algorithm for multiple source [10].

$x_1(t)$, $x_2(t)$ and $n_1(t), n_2(t)$ are received signals by sub-array and additive noise, respectively. The received signals are [3]:

$$\begin{aligned} x_1(t) &= [a(\mu_1), \dots, a(\mu_d)]s(t) + n_1(t) \\ &= As(t) + n_1(t) \end{aligned} \quad (2.33a)$$

$$\begin{aligned} x_2(t) &= [a(\mu_1)e^{j\mu_1}, \dots, a(\mu_d)e^{j\mu_d}]s(t) + n_2(t) \\ &= A\Phi s(t) + n_2(t) \end{aligned} \quad (2.33b)$$

where d: number of sources impinging on the array, $A = [a(\mu_1), \dots, a(\mu_d)]$: $n \times d$ steering matrix of the sub-array, $s(t)$: the signal received by the first sub-array,

$\Phi = \text{diag} [e^{j\mu_1}, \dots, e^{j\mu_d}]$: rotational operator, refers to the delay between the sub-array and $\mu_i = -\frac{2\pi f_c}{c} \Delta \sin \theta_i = -\frac{2\pi}{\lambda} \Delta \sin \theta_i$

After the combination of Eq. (2.33a) and Eq. (2.33b), total received signal by the system can be expressed as:

$$x(t) = \begin{bmatrix} x_1(t) \\ x_2(t) \end{bmatrix} = \begin{bmatrix} A \\ A\Phi \end{bmatrix} s(t) + \begin{bmatrix} n_1(t) \\ n_2(t) \end{bmatrix} = \tilde{A}s(t) + n(t) \quad (2.34)$$

Estimating DOA by using ESPRIT relies on determining subspace rotational operator and then estimation of μ_i . In the absence of noise, the covariance matrix of the received signal can be expressed as:

$$R_{xx} = E[x(t)x^H(t)] = \tilde{A}R_{ss}\tilde{A}^H \quad (2.35)$$

Assume that there is a matrix E_s spans the signal subspace which is also spanned by \tilde{A} . Consequence of this $\text{Range}\{E_s\} = \text{Range}\{\tilde{A}\}$ relationship, E_s and \tilde{A} can be related through unique non-singular matrix T.

$$E_s = \tilde{A}T \quad (2.36)$$

After the decomposition of E_s into two sub-array:

$$E_s = \begin{bmatrix} E_1 \\ E_2 \end{bmatrix} = \begin{bmatrix} AT \\ A\Phi T \end{bmatrix} \quad (2.37)$$

Because of their identical configuration, it can be easily said that both sub-array of the E_s have the same dimensions and span the same space as follows:

$$\text{Range}\{E_1\} = \text{Range}\{E_2\} = \text{Range}\{A\} \quad (2.38)$$

Based on the feature above, a non-singular $d \times d$ matrix Ψ can be associated with sub-array of E_s as follows [1,3]:

$$E_1\Psi = E_2 \rightarrow AT\Psi = A\Phi T \quad (2.39)$$

$$\Psi = T^{-1}\Phi T \leftrightarrow \Phi = T\Psi T^{-1} \quad (2.40)$$

According to the equations above, it is clear that the Eigen-values of Ψ is equal to the diagonal of Φ and the eigenvectors of Ψ is equal to the columns of T . As a result, the angles of arrival can be computed after computation of Eigen-values of Ψ . The summarized algorithm can be seen in Figure 2.6.

The DOA estimation equations above are available in the absence of noise, but in practical situations, an additive noise is received by the system and the covariance matrix in Eq. (2.35) takes the form of:

$$R_{xx} = E[x(t)x^H(t)] = \tilde{A}R_{ss}\tilde{A}^H + \sigma_N^2 I_{2n} \quad (2.41)$$

Therefore, $\text{Range}\{E_s\} \neq \text{Range}\{\tilde{A}\}$, $\text{Range}\{E_1\} \neq \text{Range}\{E_2\}$ and $E_1\Psi = E_2$ is no longer exactly satisfied [3,10,11]. To estimate the accurate value of Ψ , Least Square ($\hat{X} = [AA^H]^{-1} A^H B$) and Total Least Square ($[A + R_A]\hat{X} = B + R_B$) Techniques are generally employed.

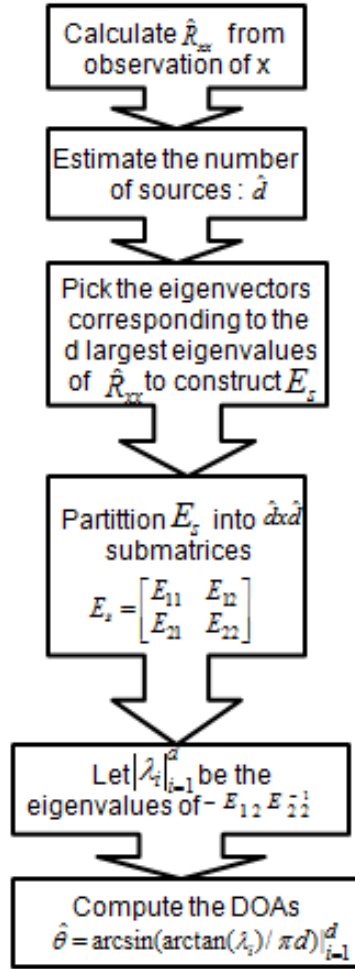


Figure 2.6: The steps of ESPRIT Algorithm

2.2.3 The maximum likelihood techniques

The Maximum Likelihood (ML) techniques provide better performance than subspace algorithms, but they aren't preferred due to computational complexity. These techniques work even in multipath environment [1].

The basic principal of the algorithm is the reconstruction of the incident signal vector from array output vector [1, 13]. The array output vector of r incident signals is as follows:

$$x(t) = A(\theta)s(t) + n(t) \quad (2.42)$$

where $\theta = [\theta_0, \theta_1, \dots, \theta_{r-1}]$, $A(\theta)$: array response, $s(t)$: incident signal vector and $n(t)$: an additive noise vector

The reconstruction method is that subtraction ($A(\hat{\theta})\hat{s}_i$) from the array output vector $x(t_i)$. The joint probability function of x can be expressed as [6]:

$$f(x) = \prod_{i=0}^{N-1} \frac{1}{\pi \det(\sigma^2 I)} \exp\left(-\frac{1}{\sigma^2} |x_i - A(\theta_i)s_i|^2\right) \quad (2.43)$$

where x_i : i th column of the array output vector

Ignoring the constant terms, the log likelihood function is:

$$L = -Nr \log \sigma^2 - \frac{1}{\sigma^2} \sum_{i=0}^{N-1} |x_i - A(\theta_i)s_i|^2 \quad (2.44)$$

Maximization of L by the unknown parameters s and θ equals to minimization equation below [1, 6].

$$\min_{\theta_k, s} \left\{ \sum_{i=0}^{N-1} |x_i - A(\theta_i)s_i|^2 \right\}$$

(2.45)

The solution of the minimization function only in terms of s by fixing θ is[1]:

$$s_i = \left(A^H(\theta_i)A(\theta_i) \right)^{-1} A^H(\theta_i)x_i \quad (2.46)$$

2.3 Summary

This chapter presents background on array processing and direction of arrival techniques. Three types of DOA techniques are described in the order; Classical methods: Delay and Sum method and Capon algorithm; Subspace methods: MUSIC, The Root-MUSIC Algorithm, The Minimum Norm Method and ESPRIT; and Maximum Likelihood (ML) method.

The classical methods are inferior to subspace methods and Maximum Likelihood technique. The performance of ML is better than subspace methods, but the computational complexity is the drawback of this method. A 2D direction finding system will be introduced in the next chapter and an alternative version of MUSIC algorithm is used for DOA estimation.

3. 2D DIRECTION FINDING SYSTEM AND RECALIBRATION OF THE ARRAY

This chapter will describe a 2D direction finding system in detail and a recalibration technique for the antenna array of this system will be proposed.

3.1 2D Direction Finding System

The 2D direction finding system for backscatter-tag's identification and localisation is designed by the authors of [14]. The system includes Uniform Circular Array (UCA) with 8 sensors, commercial reader to communicate with one single tag, RF/BF circuits to obtain In-phase and Quadrature (I&Q) signal from the output signal of the array and Digital Signal Processing (DSP) where the Direction of Arrival technique is applied. The schematic diagram of the system can be seen in Figure 3.1 and each block of the system will be briefly examined in the sub-sections.

3.1.1 Uniform circular array

The physical characteristic of the antenna array will be explained in this section. The array is an 8-sensors Uniform Circular Array and mounted on a hexagonal metal plate with 0.3m radial (see Figure 3.2). The frequency band of the array is appropriate for European UHF RFID band (868-870 MHz) [15].

Each sensor of the array is a miniaturized slot antenna printed on a non-resonating metallic box and fed by a thin stripline. The metallic box is chosen because it can be reconfigured easily and it both lowers the back radiation and allows keeping an acceptable bandwidth at the same time [15]. The total volume of one slot is equal to $(0.25\lambda_0 \times 0.25\lambda_0 \times 0.03\lambda_0)$. A slotted-box sensor illustration can be seen in Figure 3.3.

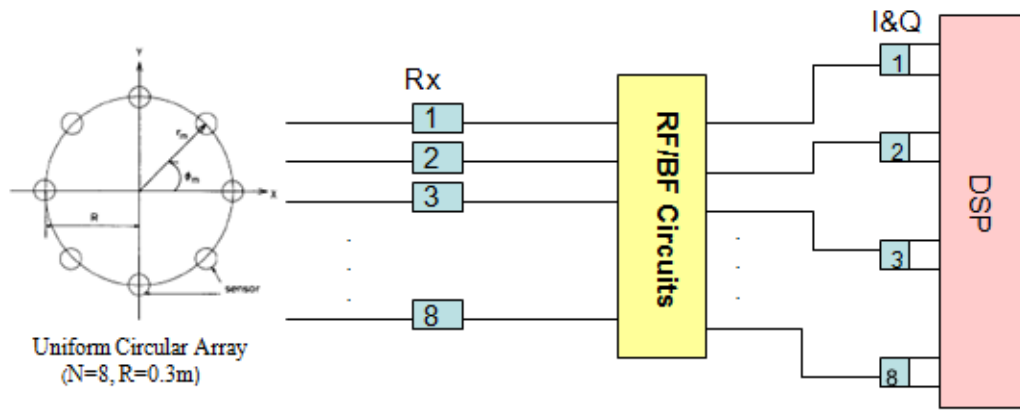


Figure 3.1: Schematic diagram of 2D direction finding system

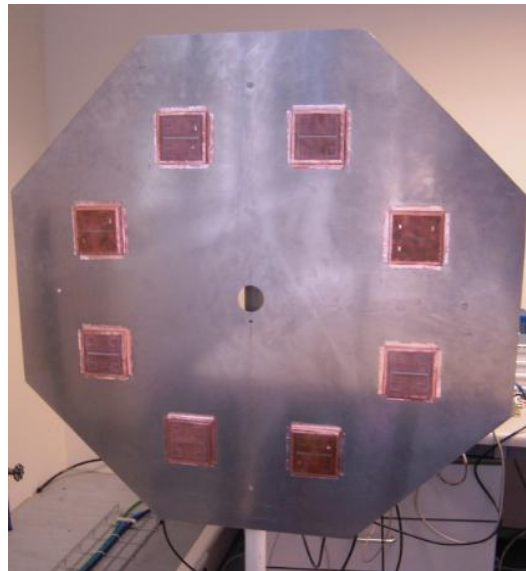


Figure 3.2: Uniform Circular Array with 8 slotted-box antennas

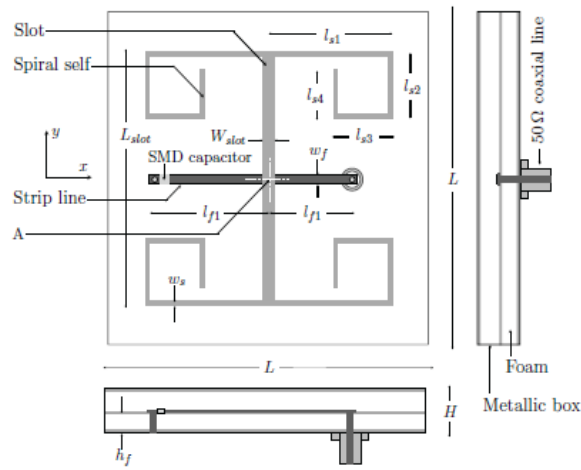


Figure 3.3: A slotted-box sensor with parameters: $H=10\text{mm}$, $h_f= 5\text{mm}$, $\lambda = 344.8\text{mm}$, $L= 86\text{mm}$, $l_{f1}= 36\text{mm}$, $l_{f2}=39\text{mm}$, $L_{slot}= 63\text{mm}$, $l_{s1}=30\text{mm}$, $l_{s2}= 16.7\text{mm}$, $l_{s3}=14.4\text{ mm}$, $l_{s4}= 12.5\text{ mm}$, $w_f=1.5\text{mm}$, $w_s=0.75\text{mm}$, $W_{slot}=3\text{mm}$ [15].

3.1.2 RF/BF circuits of the direction finding system

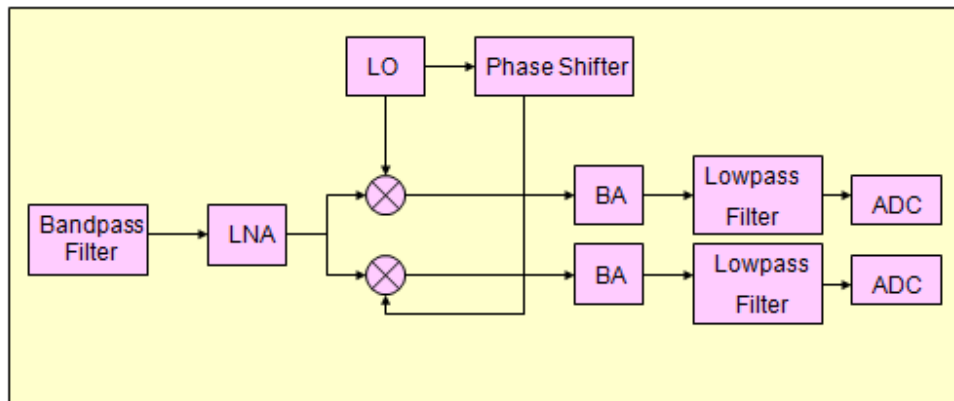


Figure 3.4: RF/BF Circuits' block diagram

The basic concept of the operation shown in Figure 3.4 is as follows. The RF signal obtained from the array is filtered in the Band-pass Filter stage, thus the signals which are at the undesired frequency band levels are discarded. The filtered signal is amplified in the Low Noise Amplifier (LNA). The demodulator converts the signal to baseband (down-converted) in I&Q signal, then the signal amplified in the Baseband Amplifier (BA) and the output of the Low-pass Filter has only the baseband component. At the last stage, the analogue baseband signal is converted to digital signal by Analogue/Digital Converter (ADC).

3.1.3 Digital signal processing (DSP)

To communicate with a tag, a commercial reader, dipole antenna which works both as a transmitter and also as a receiver and user interface program are needed.

The reader uses dipole antenna to transmit RF signal which includes the query for all tags in dipole's coverage area. The passive tags receive that signal and respond the query by using the power of the received signal. Then the reader receives this responds via dipole and sends another query with respect to given respond. Therefore, a query-respond circle and continuous communication between reader and tags are occurred. A communication example between the reader (interrogator) and a tag can be seen in Figure 3.5.

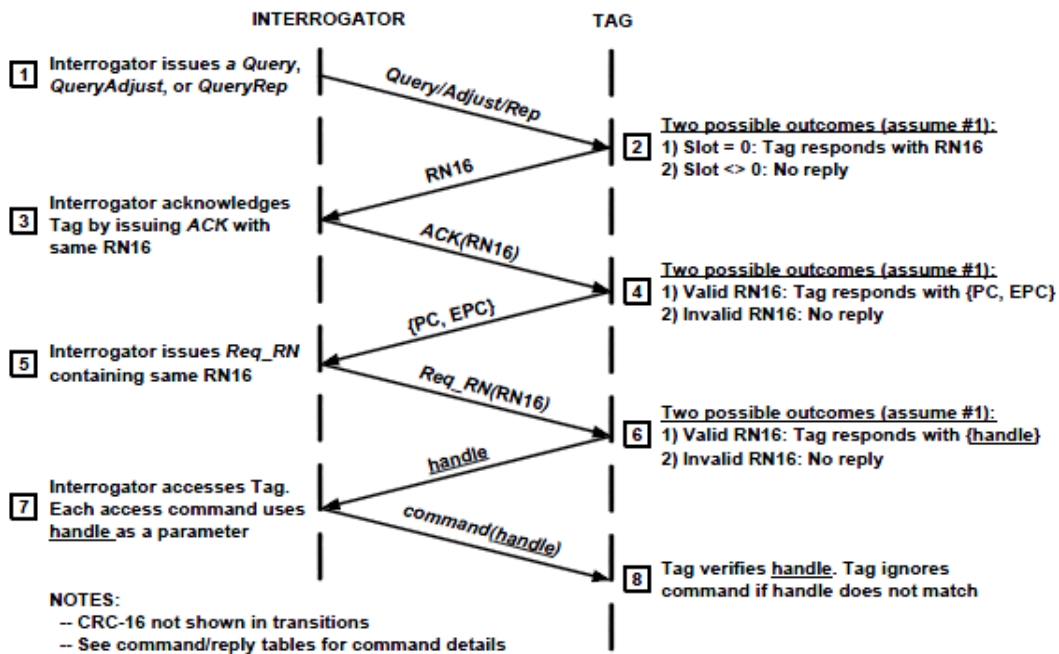


Figure 3.5: A reader-tag communication example [16]

The list of tags talking to reader at the moment is shown by the user interface program. This program allows selecting one tag to track and killing the other tags while tracking the selected. The signals coming from the dipole and the selected tag are received by the array and after passing RF/BF circuits, I&Q signals arrives at the personal computer where the digital signals are going to be processed.

This digital signals consist of 8x(I&Q) signals, therefore they arrive at the computer through 16 channels. Each (I&Q) signal pairs are combined to obtain the data received by each array sensor and then passed through high pass filter to avoid the

capacitive ramp effect of the signal. Since the dipole is an active and the tag is a passive RF source, the received signal level obtained through the dipole is much higher than the signal coming from the tag. To isolate the tag's signal, the filtered signal's continuous lower voltage level blocks are taken as a tag data. The continuous signal is searched because the tag responds the query in binary and this causes a continuous sequence. The spatial covariance matrix is computed from the estimated tag data and MUSIC algorithm is applied as a DOA technique to find the position of the tag.

As mentioned in section 2.2.2.1, the next steps of the MUSIC are performing Eigen decomposition of the covariance matrix, forming the steering vector for all possible angles in u-v space and computing the power from Eq. 3.1, picking the largest peak in the power spectrum and finding the position of the tag. The power equation for MUSIC algorithm used in the computer program in terms of k is as follows [17].

$$P(\bar{k}) = \frac{1}{\bar{e}(\bar{k})^H \bar{U}_N \bar{U}_N^H \bar{e}(\bar{k})} \quad (3.1)$$

where $\bar{e}(\bar{k})$: a column vector of phase delay of the antenna array and M=the array's element number,

$$e = \begin{bmatrix} \exp(j\bar{k}\bar{r}_1) \\ \exp(j\bar{k}\bar{r}_2) \\ \vdots \\ \exp(j\bar{k}\bar{r}_M) \end{bmatrix} \quad (3.2)$$

^H: Hermitian transpose, \bar{U}_N :the matrix of noise subspace eigenvector

3.2. Array Recalibration of the Direction Finding System

This section has two parts. In the first part, the array calibration and calibration method used will be explained and then a new recalibration technique will be proposed in the second section.

3.2.1 Array calibration

The phase and amplitude mismatch between array sensors and mismatch between array cables have a remarkable effect on beamforming and direction finding systems. Calibrating the array to overcome this problem is very critical for system accuracy [18, 19]. There have been lots of calibration methods proposed over few decades. Some of the most preferred methods exploit the signal information coming from known direction in order to use it as a calibration data, but in practice, the information is sometimes unfavourable. There is another way to calibrate the array called self-calibration. The self-calibration methods' downsides are that they are very time-consuming and have varied ambiguity issues although they don't need any calibration sources [20].

The array calibration methods which exploit the signal information coming from known direction will be examined and they can be sorted in three groups as [18]:

- 1) analytical method based on mathematical equations
- 2) numerical method based on computer simulations
- 3) experimental method based on calibration sources

The most common method is the third one; two types of experimental array calibration method will be described.

3.2.1.1 Remote transmitter approach

As it is known, the estimation of steering vector is very important for DOA techniques. In the Remote Transmitter Approach, a calibration source is located in a known place right in front of the array and the signals coming from this source are recorded and normalized while the array is rotating. These signals are used for estimating the steering vector [18]. The unpredictable multipath effects are the disadvantages of this method [19].

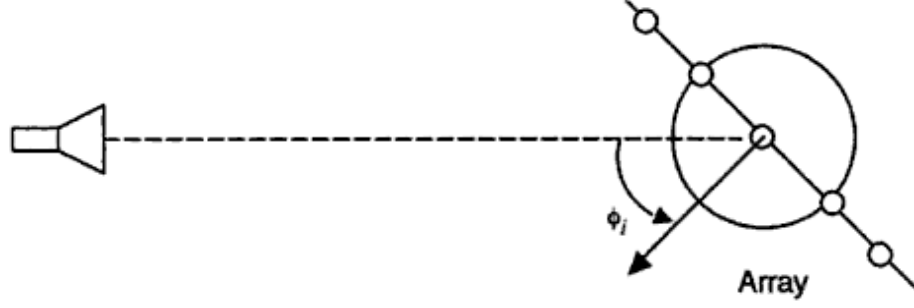


Figure 3.6: Remote Transmitter Approach [18]

3.2.1.2 Test tone approach

The Test-Tone approach is the calibration method used by the direction finding system described before. Ideally, each sensor of the array receives the same data in the presence of a calibration source in front of the array, but there are known mismatch effects on the system. Assume that the signal received by the k th sensor is x_k and the array consists of M sensors. The array output vector including mismatch effects is:

$$\begin{bmatrix} y_1(t) \\ y_2(t) \\ \vdots \\ y_M(t) \end{bmatrix} = \begin{bmatrix} c_1 \\ c_2 \\ \vdots \\ c_M \end{bmatrix} x_1(t) \quad (3.3)$$

Let $k=1$ be the reference element and the relative phase response of the element 1 with respect to the element k is denoted by r_k [18].

$$r_k = \frac{c_1}{c_k} \approx \left\langle \frac{y_1}{y_k} \right\rangle \quad (3.4)$$

If each element of the output vector is multiplied by the corresponding relative phase delay response, the mismatch effects will be compensated [18].

$$\begin{bmatrix} r_1 y_1(t) \\ r_2 y_2(t) \\ \vdots \\ r_M y_M(t) \end{bmatrix} = \begin{bmatrix} r_1 c_1 x_1(t) \\ r_2 c_2 x_2(t) \\ \vdots \\ r_M c_M x_M(t) \end{bmatrix} = c_1 \begin{bmatrix} x_1 \\ x_2 \\ \vdots \\ x_M \end{bmatrix} \quad (3.5)$$

As it is seen in Eq. (3.5), the input signals received by each sensor is normalized by the same value: c_1 , therefore the signal received by the each sensor would be the same in phase and amplitude.

In used direction finding system, the multiplier is the first row of the spatial covariance matrix ($R_{xx}(1,i)$) which is estimated from the signal coming from the tag. This is because the first row of the matrix represents the relationship of the sensors with the first (reference) sensor of the array. The steps of the used array calibration can be summarized as follows:

- 1) Placing the calibration tag (in the red circle) towards the antenna array at a certain distance as seen in Figure 3.7.
- 2) Estimating the spatial covariance matrix from the raw data coming from the calibration tag.
- 3) Obtaining the “Calibration Vector” from the first row of the covariance matrix.

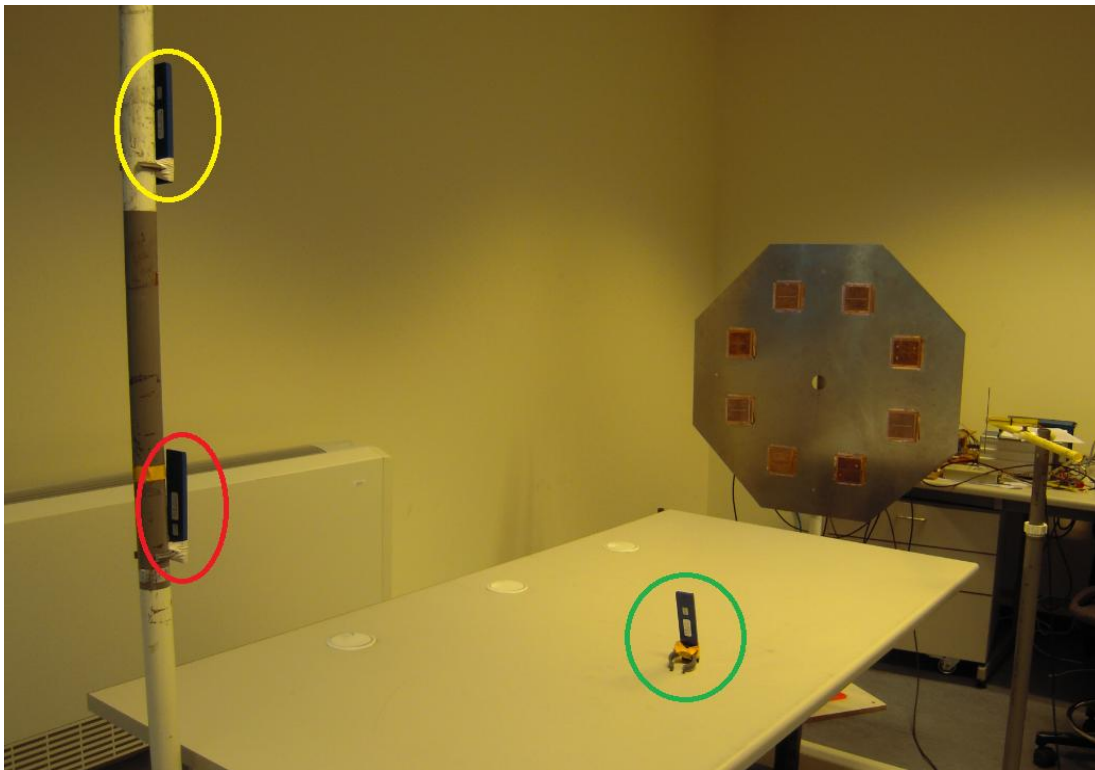


Figure 3.7: The calibration position of the system. The tag in the red circle is the calibration tag.

As seen in Figure 3.7, the calibration tag is located at the level of the array centre; therefore the signal received by the each sensor must be the same in phase and amplitude. Therefore, the calibration vector is all about the mismatch effects.

To ensure that calibration works, two more tags are placed on different places and their positions are estimated. Figure 3.8 which is a contour plot of the MUSIC pseudo power spectrum shows the estimated positions of the calibration tag in the red circle, the tag on the table (in the green circle) and the tag above the calibration tag (in the yellow circle) with respect to the centre of the array. The axes are in u-v space and the localisation results are in azimuth and elevation angles, respectively. The localization result of the calibration tag is found as [azimuth, elevation] = (10, 89.820). Let's consider the elevation angle; we know that the calibration tag is placed towards the array at the same height with the centre of array; hence the elevation and azimuth angles are expected to be around 90 and 0. Elevation angle is reasonably close to the expected value and so elevation is. Because of the elevation angle's being 90 degrees, tiny changes in elevation angle causes big angle differences. For the tag above the calibration tag, azimuth angle should be around 90 degrees and elevation should be less than 90. Lastly, for the tag on the table azimuth should be negative and elevation should be between 70-80 degrees. Therefore it can be said that the array is calibrated accurately.

3.2.2 Array recalibration

As mentioned in the earlier stage of this chapter, the array calibration with calibration source in the field is not always possible because of unpredictable multipath effects. An array of a system needs to be accurately, easily and cheaply calibrated out of the laboratory in the presence of noise and irrelevant signals. A recalibration method for this system's array will be proposed in this section.

The steps of the proposed recalibration method are:

- 1) Place the dipole antenna, which is used for communication with tag, right in front of the array very closely at the level of the array's centre (see Figure 3.9). This position of the dipole had to be accurately known. Save the first row of the covariance matrix of the dipole. Note that, all the tags must be killed in this step, the only signal source should be the dipole.

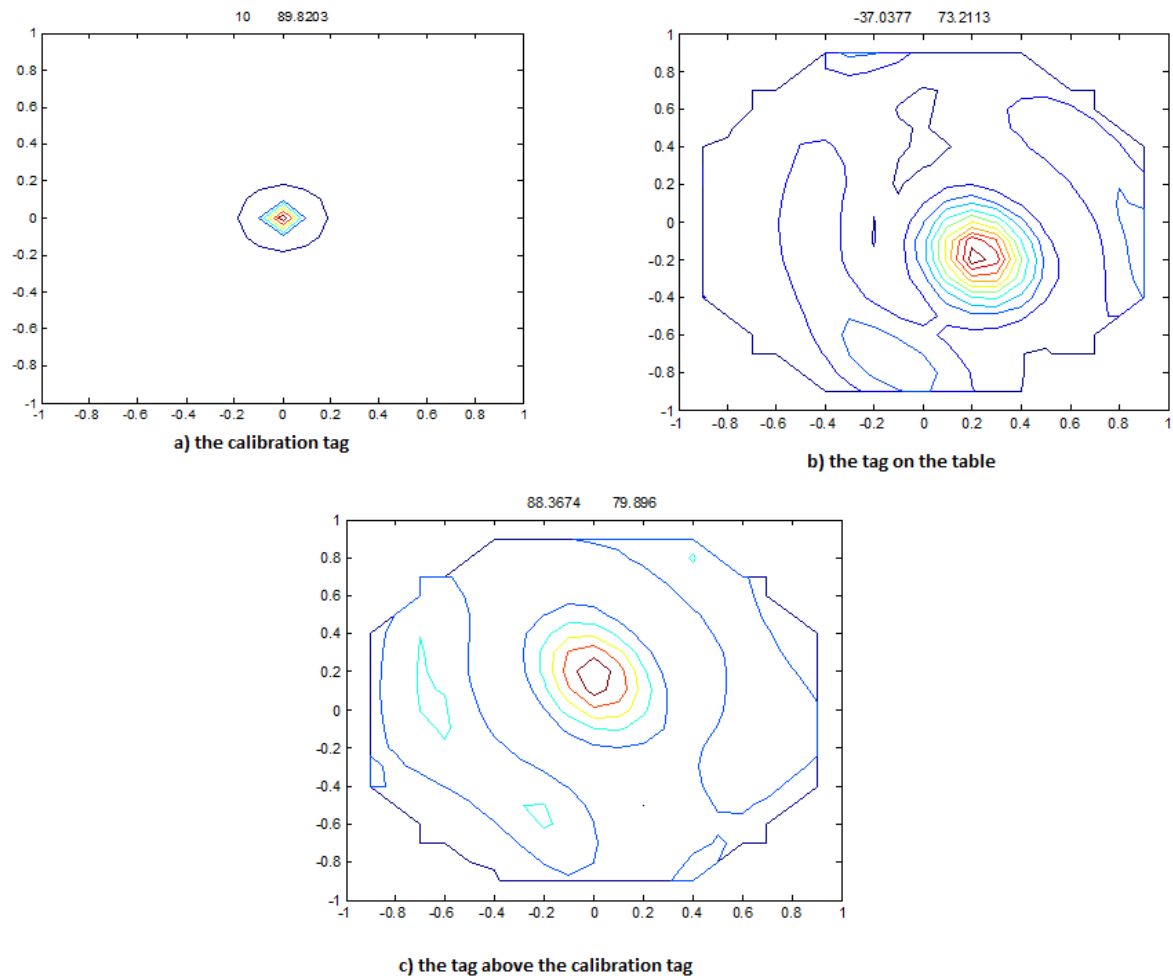


Figure 3.8: The contour plots of the estimated positions of **a)** the calibration tag (az: 10, ele: 89.820) **b)** the tag on the table (az: -37, ele. 73.211) and **c)** the tag above the calibration tag (az: 88.37, ele: 79.896)

2) Calibrate the array like explained before.

Before next step, the calibration must be destroyed. During the laboratory experiments, the calibration was ruined by randomly swapping the coaxial RF cables between the array and RF/BF circuits. This process destroys the calibration and the estimated positions of the same tags in Figure 3.7 can be seen in Figure 3.10 as a proof of ruined calibration.

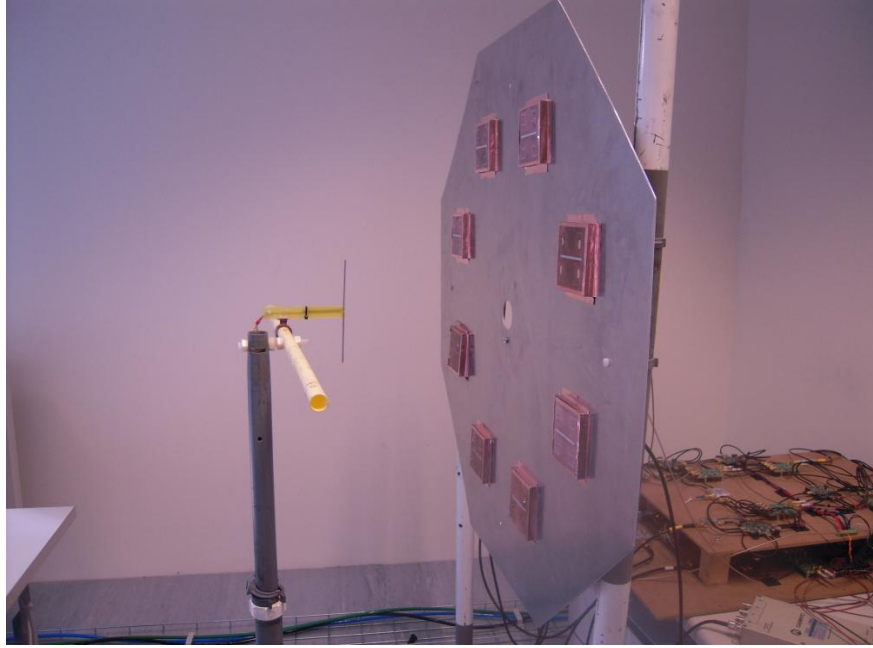


Figure 3.9: The position of the dipole in front of the array

- 3) Replace the dipole in front of the array where exactly it was placed before (see Figure 3.9). Save the first row of the covariance matrix of dipole again.
- 4) Calculate the new calibration vector as follows:

$$C_{TAG_{state2}} = C_{TAG_{state1}} * \left(\frac{first_row_of_corr_mat_{DIPOLE_{state2}}}{first_row_of_corr_mat_{DIPOLE_{state1}}} \right)^H \quad (3.6)$$

where *: element-by-element product of the vectors, ^H: Hermitian transpose

Mathematical proof:

Figure 3.11 represents the position of the array and the calibrating tag while getting the calibration matrix from the tag data. “ A_1, A_2, \dots, A_N ” are the voltages each antenna received and N is the number of sensors. “ a_1, a_2, \dots, a_N ” are the first row elements of the correlation matrix. Let’s separate the mismatch effects vector from the first row of the correlation matrix. The first row of the correlation matrix of the calibrating tag is:

$$\begin{aligned} \text{first_row_of_corr_mat}_{TAG_{state1}} &= [a_1 \quad a_2 \quad \dots \quad a_N] \\ &= [\alpha_1 \quad \alpha_2 \quad \dots \quad \alpha_N]^* [x_1 \quad x_2 \quad \dots \quad x_N] \end{aligned} \quad (3.7)$$

where

$$\begin{aligned} a_1 &= A_1 \cdot A_1^* = |A_1|^2 \\ a_2 &= A_1 \cdot A_2^* \\ &\vdots \\ a_N &= A_1 \cdot A_N^* \end{aligned}$$

$[\alpha_1 \quad \alpha_2 \quad \dots \quad \alpha_N]$: mismatch effect vector of the first state

$[x_1 \quad x_2 \quad \dots \quad x_N]$: is a constant vector, represents the first row of the correlation matrix of the calibrating tag without mismatch effect

Note that $(.)$ is the dot product of the scalar variables.

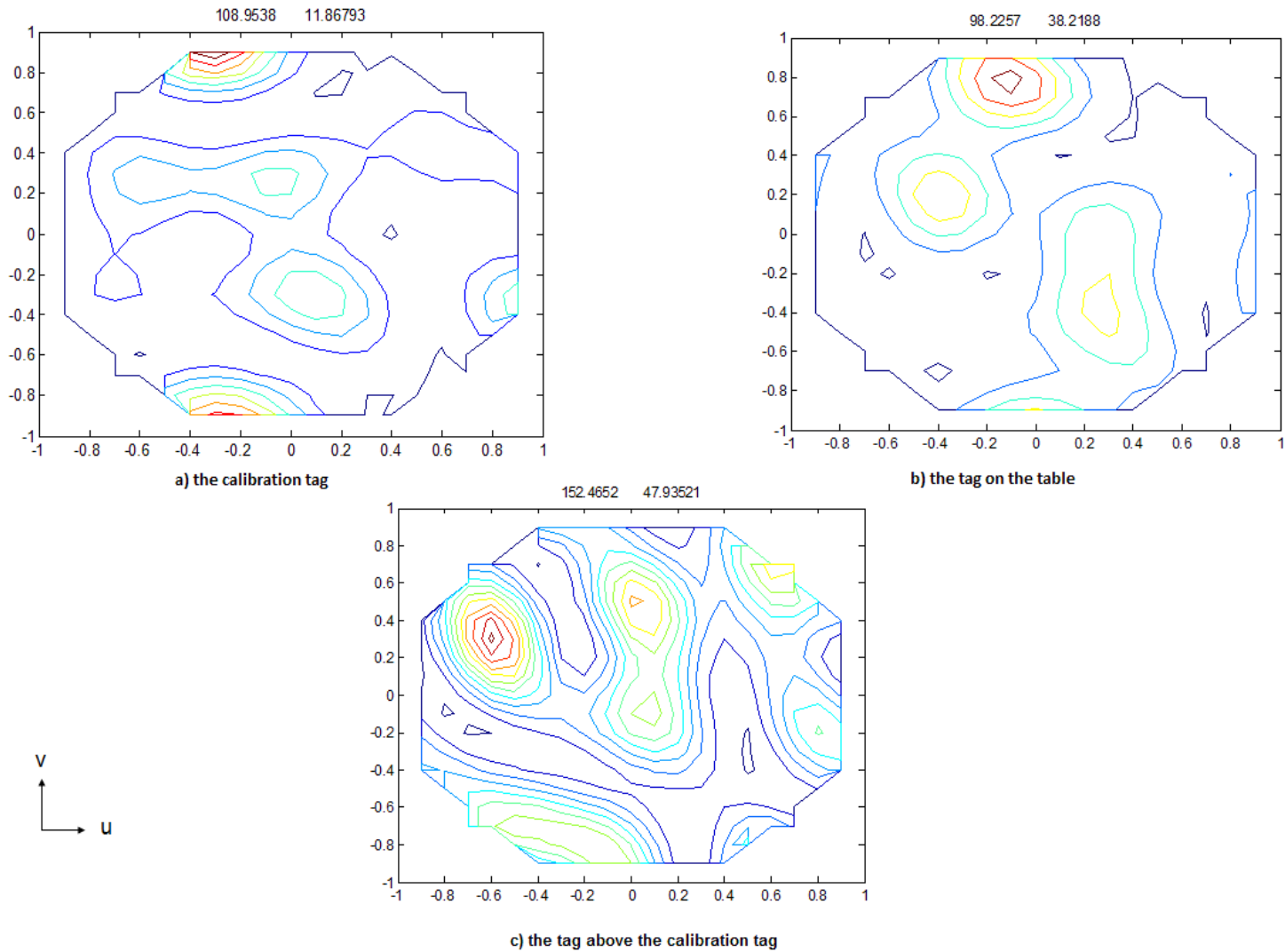


Figure 3.10: The contour plots of the estimated positions of **a)** the calibration tag (az: 108.954, ele: 11.868) **b)** the tag on the table (az: 98.226 ele: 38.219) and **c)** the tag above the calibration tag (az: 152.465, ele: 47.935).

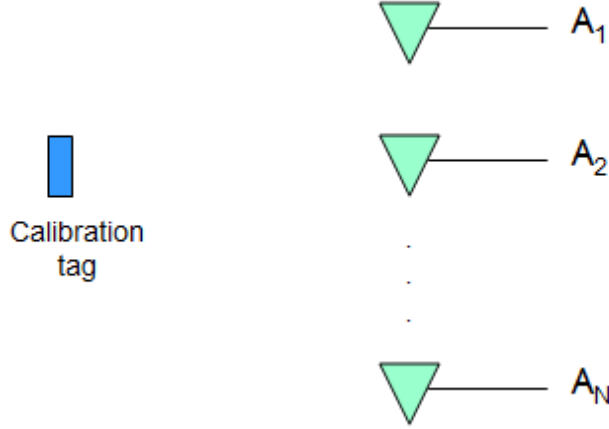


Figure 3.11: The calibrating tag and the antenna array

Calibration vector of the tag:

$$C_{TAG_{state1}} = \begin{bmatrix} a_1^* \\ a_2^* \\ \vdots \\ a_N^* \end{bmatrix} = (\bar{\alpha})^H * \begin{bmatrix} x_1^* \\ x_2^* \\ \vdots \\ x_N^* \end{bmatrix} = \begin{bmatrix} \alpha_1^* \\ \alpha_2^* \\ \vdots \\ \alpha_N^* \end{bmatrix} * \begin{bmatrix} x_1^* \\ x_2^* \\ \vdots \\ x_N^* \end{bmatrix} \quad (3.8)$$

Figure 3.12 represents the position of the array and dipole antenna while getting the calibration matrix from the dipole data. “ M_1, M_2, \dots, M_N ” are the voltages each antenna received. “ m_1, m_2, \dots, m_N ” are the first row elements of the correlation matrix. The first row of the correlation matrix is as follows:

$$\begin{aligned} first_row_of_corr_mat_{DIPOLE_{state1}} &= [m_1 \quad m_2 \quad \dots \quad m_N] \\ &= [\alpha_1 \quad \alpha_2 \quad \dots \quad \alpha_N]^* [y_1 \quad y_2 \quad \dots \quad y_N] \end{aligned} \quad (3.9)$$

where

$$\begin{aligned} m_1 &= M_1.M_1^* = |M_1|^2 \\ m_2 &= M_1.M_2^* \\ &\vdots \\ m_N &= M_1.M_N^* \end{aligned}$$

$[\alpha_1 \quad \alpha_2 \quad \dots \quad \alpha_N]$: mismatch effect vector of the first state

$[y_1 \ y_2 \ \dots \ y_N]$: is a constant vector, represents the first row of the correlation matrix of the dipole without mismatch effect

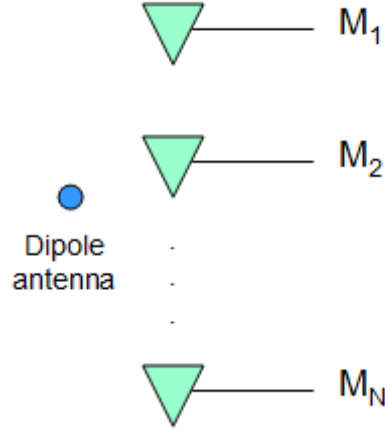


Figure 3.12: Transmitting dipole and antenna array

As mentioned before, after the destruction of the array calibration, old calibration vector didn't work anymore. On the other hand, we know the first row of the calibration matrix of the tag and dipole at the first state and the first row of the calibration matrix of the dipole at the second state; therefore we can find the new correlation vector of the tag by using these data sets.

" M'_1, M'_2, \dots, M'_N " are the voltages each antenna received from the dipole at the second state. The first row of the correlation matrix after calibration destroys is as follows:

$$\begin{aligned} \text{first_row_of_corr_mat}_{DIPOLE_{state2}} &= [m'_1 \ m'_2 \ \dots \ m'_N] \\ &= [\beta_1 \ \beta_2 \ \dots \ \beta_N]^* [y_1 \ y_2 \ \dots \ y_N] \end{aligned} \quad (3.10)$$

where

$$\begin{aligned} m'_1 &= M'_1 \cdot (M'_1)^* = |M'_1|^2 \\ m'_2 &= M'_1 \cdot (M'_2)^* \\ &\vdots \\ m'_N &= M'_1 \cdot (M'_N)^* \end{aligned}$$

$[\beta_1 \ \beta_2 \ \dots \ \beta_N]$: mismatch effect vector of the second state

$[y_1 \ y_2 \ \dots \ y_N]$: is a constant vector, represents the first row of the correlation matrix of the dipole without mismatch effect

The form of the calibration vector of the second state must be as the following equation.

$$C_{TAG_{state2}} = \begin{bmatrix} (a_1')^* \\ (a_2')^* \\ \vdots \\ (a_N')^* \end{bmatrix} = (\bar{\beta})^H * \begin{bmatrix} x_1^* \\ x_2^* \\ \vdots \\ x_N^* \end{bmatrix} = \begin{bmatrix} \beta_1^* \\ \beta_2^* \\ \beta_3^* \\ \beta_4^* \end{bmatrix} * \begin{bmatrix} x_1^* \\ x_2^* \\ \vdots \\ x_N^* \end{bmatrix} \quad (3.11)$$

The calibration vector of the second state can be expressed in terms of the calibration vector for the first state, the first row of the correlation matrix of the dipole for the first and second state as follows:

$$\begin{aligned} C_{TAG_{state2}} &= C_{TAG_{state1}} * \left(\frac{\text{first_row_of_corr_mat}_{DIPOLE_{state2}}}{\text{first_row_of_corr_mat}_{DIPOLE_{state1}}} \right)^H \\ &= C_{TAG_{state1}} * \left(\frac{\begin{bmatrix} m_1' & m_2' & \dots & m_N' \end{bmatrix}}{\begin{bmatrix} m_1 & m_2 & \dots & m_N \end{bmatrix}} \right)^H \end{aligned} \quad (3.12)$$

If the Eq. (3.12) is rewritten in terms of Eq. (3.9) and Eq. (3.10), the Eq. (3.11) will be obtained.

$$\begin{aligned} C_{TAG_{state2}} &= \begin{bmatrix} \alpha_1^* \\ \alpha_2^* \\ \vdots \\ \alpha_N^* \end{bmatrix} * \begin{bmatrix} x_1^* \\ x_2^* \\ \vdots \\ x_N^* \end{bmatrix} * \left(\frac{\begin{bmatrix} \beta_1 & \beta_2 & \dots & \beta_N \end{bmatrix} * [y_1 \ y_2 \ \dots \ y_N]}{\begin{bmatrix} \alpha_1 & \alpha_2 & \dots & \alpha_N \end{bmatrix} * [y_1 \ y_2 \ \dots \ y_N]} \right)^H \\ &= \begin{bmatrix} \alpha_1^* \\ \alpha_2^* \\ \vdots \\ \alpha_N^* \end{bmatrix} * \begin{bmatrix} x_1^* \\ x_2^* \\ \vdots \\ x_N^* \end{bmatrix} * \begin{bmatrix} (\beta_1 / \alpha_1)^* \\ (\beta_2 / \alpha_2)^* \\ \vdots \\ (\beta_N / \alpha_N)^* \end{bmatrix} = \begin{bmatrix} \beta_1^* \\ \beta_2^* \\ \vdots \\ \beta_N^* \end{bmatrix} * \begin{bmatrix} x_1^* \\ x_2^* \\ \vdots \\ x_N^* \end{bmatrix} \end{aligned} \quad (3.13)$$

As shown in Figure 13, the recalibrated system works as it should be. The localization results of the same three tags with calibrated system in the laboratory and with recalibrated system (simulated field case) are very similar; therefore the

proposed recalibration method is successful. The localization figures of the tags in Figure 3.7 are very sharp and there are no side lobe effects on the graph. The localization figures of the tags in Figure 3.13 have slight side lobe effects. Because of the fact that recalibration method depends on the dipole data, these are expected effects.

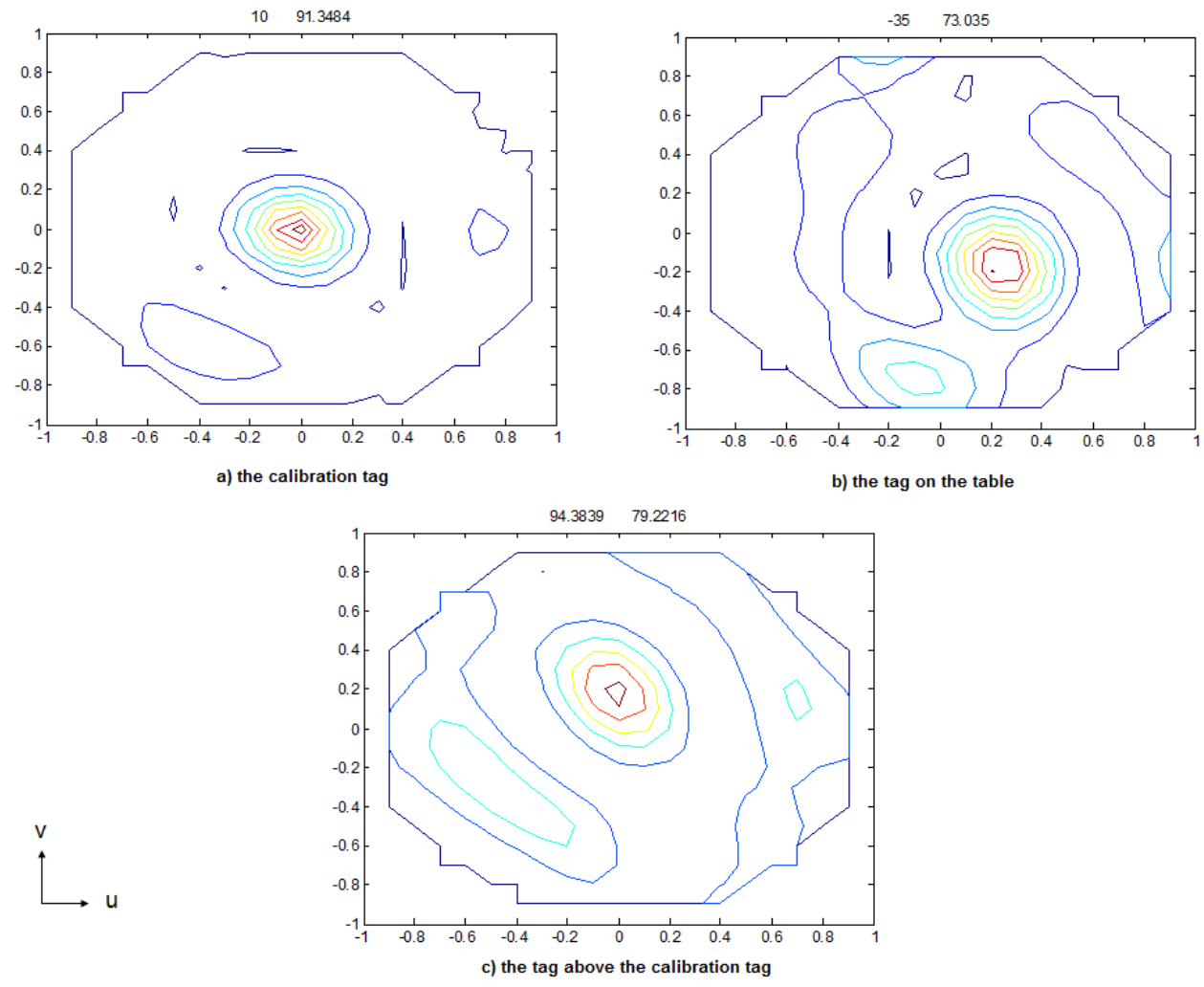


Figure 3.13: The contour plots of the estimated positions of **a)** the calibration tag (az: 10, ele: 91.348) **b)** the tag on the table (az: -35, ele: 73.035) **c)** the tag above the calibration tag (az: 94.384, ele: 79.222).

4. DOA ESTIMATION of PASSIVE RFID TAGS in MULTIPATH ENVIRONMENT

A direction finding system for passive RFID tags is introduced in the previous chapter. As mentioned before, MUSIC algorithm which is a subspace DOA estimation technique based on Eigen-decomposition is used for signal processing due to its computation simplicity. However, subspace based algorithms don't work when the signals are coherent or highly correlated in the multipath environment. To overcome this problem, a pre-processing technique called "Spatial Smoothing" which essentially "de-correlates" the signals was proposed by Evans *et al.* [21].

This chapter presents an introduction to spatial smoothing technique, an array interpolation technique to harmonize the antenna array against the constraints of the spatial smoothing and an iterative spatial smoothing algorithm proposed by Hislop and Craeye [22].

4.1 Spatial Smoothing

In this section, problem statement and spatial smoothing algorithm will be presented.

4.1.1 Problem statement

Assume that DOA system has a uniform linear array with N identical antennas and q ($N > q$) signals coming from $\{\theta_1, \theta_2, \dots, \theta_q\}$ are received by the array. The signal impinged on the sensors is:

$$x(t) = As(t) + n(t) \tag{4.1}$$

where $A = [a(\theta_1), \dots, a(\theta_q)]$: $N \times q$ matrix whose columns are composed of steering vectors in the direction of incoming signals, $s(t) = [s_1(t), \dots, s_q(t)]^T$: $q \times 1$ incoming signals vector and $n(t)$: $q \times 1$ additive noise vector whose elements' variance are considered identical.

The additive noises are also considered as uncorrelated with the signals and uncorrelated between themselves. The basic condition of the subspace based DOA estimation algorithms is that the data covariance matrix must be full rank. The covariance matrix is:

$$R_{xx} = E[x(t)x^H(t)] = AR_{ss}A^H + \sigma^2 I_{N \times N} \quad (4.2)$$

The full rank condition depends on the signal covariance matrix R_{ss} . If the signals are uncorrelated, R_{ss} has full rank q , it is diagonal and non-singular. It is non-diagonal and non-singular if the signals are partially correlated; non-diagonal and singular if some of the signals are fully correlated (coherent) [23]. When the signals are uncorrelated, Eigen-values and corresponding eigenvectors of R_{xx} are as follows [23-25]:

$$\{\lambda_1 \geq \lambda_2 \geq \dots \geq \lambda_N\} \text{ and } \{v_1, v_2, \dots, v_N\} \quad (4.3)$$

the rank properties mean that[23-25]:

- 1) $N-q$ minimum Eigen-values of R_{ss} are equal to σ^2

$$\lambda_{q+1} = \lambda_{q+2} = \dots = \lambda_N = \sigma^2 \quad (4.4)$$

- 2) The corresponding eigenvectors of the $N-q$ minimum Eigen-values are orthogonal to the matrix A whose columns are composed of the steering vectors.

$$\{v_{q+1}, v_{q+2}, \dots, v_N\} \perp \{a(\theta_1), \dots, a(\theta_q)\} \quad (4.5)$$

The subspace based DOA estimation algorithms base on these two properties and the properties above are provided if only R_{ss} is non-singular. Assume that the first two of the impinging signals are coherent. The total incoming signal and the relation of the coherent signals are as follows [25]:

$$s_2(t) = \alpha s_1(t) \quad (4.6)$$

where α : complex scalar

$$x(t) = \tilde{A}\tilde{s}(t) + n(t) \quad (4.7)$$

where $\tilde{A} = [a(\theta_1) + \alpha a(\theta_2), a(\theta_3), \dots, a(\theta_q)]$: $N \times (q-1)$ steering vector matrix and $\tilde{s}(t) = [(\alpha + 1)s_1(t), \dots, s_q(t)]^T$: $(q-1) \times 1$ incoming signal vector.

In that case Eq. (4.2) becomes:

$$R_{xx} = E[x(t)x^H(t)] = \tilde{A}\tilde{R}_{ss}\tilde{A}^H + \sigma^2 I \quad (4.8)$$

where $\tilde{R}_{ss} = E[\tilde{s}(t)\tilde{s}^H(t)]$: the signal correlation matrix

The signal correlation matrix is still non-singular and has $(q-1) \times (q-1)$ rank; the steering vector matrix \tilde{A} is a full column rank. Therefore, the properties above can be rewritten as [23-25]:

- 1a) $N - (q-1)$ minimum Eigen-values of \tilde{R}_{ss} are equal to σ^2
- 2a) The corresponding eigenvectors of the $N - (q-1)$ minimum Eigen-values are orthogonal to the matrix \tilde{A} whose columns are composed of the steering vectors.

Since the first element of the matrix \tilde{A} related to the first two coherent signals is $a(\theta_1) + \alpha a(\theta_2)$, only $(q-2)$ angles of arrival can be resolved accurately. In general, $(q-p)$ directions of arrival can be estimated if the number of the coherent signals is p .

4.1.2 Spatial smoothing algorithm

As mentioned in the previous chapter, the accuracy of the subspace based DOA estimation algorithm associated with the non-singularity property of the signal correlation matrix. The spatial smoothing technique de-correlates the signals and generates a non-singular signal correlation matrix from the raw data.

Spatial smoothing technique is only applicable to linear uniformly spaced arrays. The basic principle of the technique is dividing the array into sub-arrays (see Figure 4.1) and computing the non-singular signal correlation matrix by averaging the signal correlation matrixes obtained from each sub-arrays.

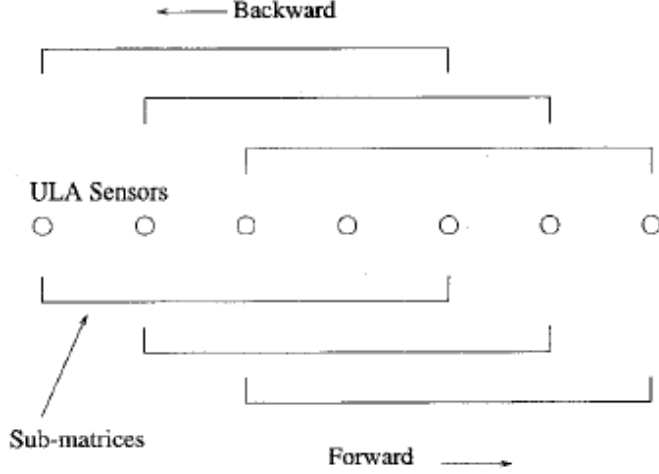


Figure 4.1: Sub-array spatial smoothing [27]

Assume that a Uniform Linear Array (ULA) composed of N sensors is divided into K sub-arrays and the displacement between the sensors is d . The sensor number of each overlapping sub-arrays is N_0 , such as the elements of the first and second sub-arrays are $\{1, 2, \dots, N_0\}$ and $\{2, 3, \dots, N_0 + 1\}$, respectively. The received signal by the k th sub-array is denoted by [25]:

$$x_k(t) = \hat{A}D_k s(t) + n_k(t) \quad (4.9)$$

where $D_k = \text{diag}\{e^{j\pi d(k-1)\sin\theta_1}, \dots, e^{j\pi d(k-1)\sin\theta_q}\}$: $q \times q$ diagonal matrix

The covariance matrix of the k th sub-array is [25]:

$$R_{xx_k} = E[x_k(t)x_k^H(t)] = \hat{A}D_k R_{ss} D_k^H \hat{A}^H + \sigma^2 I \quad (4.10)$$

The average of the sub-array covariance matrixes is:

$$\bar{R}_{xx} = \frac{1}{K} \sum_{k=1}^K R_k \quad (4.11)$$

where $K = N - N_0 + 1$: the number of sub-array

\bar{R}_{xx} is defined as spatially smoothed covariance matrix. Combining Eq. (4.11) with Eq. (4.10), the spatially smoothed covariance matrix can be written as:

$$\begin{aligned}\bar{R}_{xx} &= \hat{A} \left(\frac{1}{K} \sum_{k=1}^K D_k R_{ss} D_k^H \right) \hat{A}^H + \sigma^2 I \\ &= \hat{A} \bar{R}_{ss} \hat{A}^H + \sigma^2 I\end{aligned}\quad (4.12)$$

Where spatially smoothed covariance matrix of the signal:

$$\bar{R}_{ss} = \frac{1}{K} \sum_{k=1}^K D_k R_{ss} D_k^H \quad (4.13)$$

As long as the number of the sub-array is larger than the signals (e.g. $K > q$), spatially smoothed signal covariance matrix is non-singular and suitable for MUSIC algorithm.

The technique explained above is called forward spatial smoothing. To estimate DOA of q signals, each sub-array must have at least $(q+1)$ sensors and the total number of the sensors in the array must be $2q$. An alternative spatial smoothing technique called Forward/Backward Spatial Smoothing which increases the sub-array size to $2K$ without changing the array size was proposed by the authors of [26]. In this technique, the array is divided into K sub-array in both forward and backward directions (see Figure 4.1), thus the required array size decreases to $3q/2$.

The average covariance matrix consisting of forward and backward covariance matrixes is [27]:

$$\begin{aligned}R_{ssave} &= \frac{1}{2} (\bar{R}_{ssforward} + \bar{R}_{ssbackward}) = \frac{1}{2} (\bar{R}_{ss} + J \bar{R}_{ss}^* J) \\ &= \frac{1}{2} \left(\bar{R}_{ss} + \begin{bmatrix} 0 & \dots & 0 & 1 \\ 0 & \dots & 1 & 0 \\ \vdots & \ddots & \vdots & \vdots \\ 1 & \dots & 0 & 0 \end{bmatrix} \bar{R}_{ss}^* \begin{bmatrix} 0 & \dots & 0 & 1 \\ 0 & \dots & 1 & 0 \\ \vdots & \ddots & \vdots & \vdots \\ 1 & \dots & 0 & 0 \end{bmatrix} \right)\end{aligned}\quad (4.14)$$

The forward-backward covariance matrix is [27]:

$$\bar{R}_{xx}^{fb} = \hat{A} \bar{R}_{ssave} \hat{A}^H + \sigma^2 I \quad (4.15)$$

The steps of DOA estimation of coherent signals can be seen in Figure 4.2.

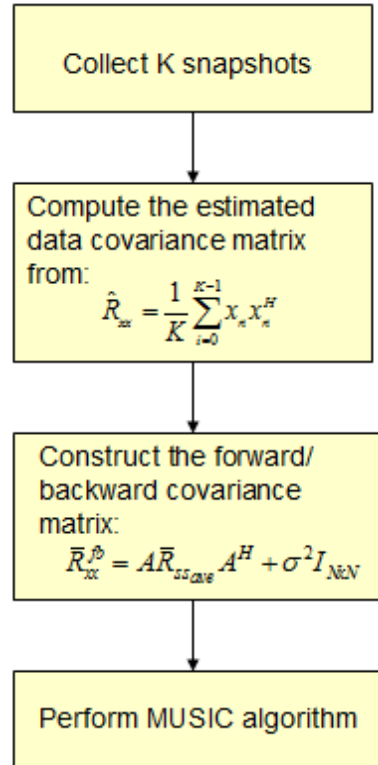


Figure 4.2: Block diagram of DOA estimation of coherent signals

4.2 The Interpolated Array Technique

Spatial smoothing techniques can be applied only linear uniformly spaced arrays such as ULAs. Since ULAs' array response vectors having a Vandermonde form, they have received most attention. On the other hand, these types of arrays are not preferred in practical applications because provided coverage area in azimuth plane is less than 360° . In practice, efficient DOA estimation systems should provide both 360° coverage and accurate resolution of the coherent signals. A planar array such as UCA instead of ULA should be used to overcome coverage problem and a pre-processing technique called array interpolation should be applied to generalize the spatial smoothing for planar arrays [28].

Estimating the array response of the virtual array from that of the real array is the main role of the interpolated arrays. Linear array interpolation techniques have been used for this purpose. The covariance matrix estimation of the interpolated virtual array steps are as follows [25]:

- 1) The coverage area (the field of view) of the array should be separated properly. The interval of the each sector can be shown as $[\theta_i^1, \theta_i^2]$; for instance, the interval of the first sector is $[0, 45]$ when the 360° coverage area is divided into 8 sectors.
- 2) The step size for each interval should be determined to generate a set of angles to design the interpolation matrix.

$$\Theta_i = [\theta_i^1, \theta_i^1 + \Delta\theta, \theta_i^1 + 2\Delta\theta, \dots, \theta_i^2] \quad (4.16)$$

- 3) Compute the steering vector matrix from the set of angles generated in the previous step. The steering vector matrix below is associated with the real array.

$$A_i = [a(\theta_i^1), \dots, a(\theta_i^2)] \quad (4.17)$$

An array manifold of the virtual array, in other words array response of the virtual array is:

$$\bar{A}_i = [\bar{a}(\theta_i^1), \dots, \bar{a}(\theta_i^2)] \quad (4.18)$$

- 4) The key idea of the array interpolation is obtaining the virtual array manifold by using the linear interpolation of the real array manifold.

$$B_i A_i = \bar{A}_i \quad (4.19)$$

where B_i is a constant matrix.

The least square estimation of the constant matrix is [29]:

$$B_i = (A_i A_i^H)^{-1} A_i \bar{A}_i^H \quad (4.20)$$

- 5) This step is a decision step for accommodation of the sector interval. If the Frobenious norm of $(\bar{A}_i - B_i A_i)$ is small enough with respect to the Frobenious norm of \bar{A}_i , a virtual array is interpolated accurately. If not, go back to step one and reduce the size of the sector.

After obtaining the interpolation matrixes, the covariance matrix of the virtual array can be computed as follows [25]:

$$R_i = B_i R B_i^H \quad (4.21)$$

4.3 Iterative Spatial Smoothing Algorithm for 2D Direction Finding

In practical applications of the 2D direction finding system described in Chapter 3, some problems caused by environment and design might be seen. An iterative spatial smoothing algorithm included array interpolation for 2D sensing was proposed by Hislop and Craeye as a solution. The steps of the algorithm are [22]:

- 1) Obtain the steering vector matrix of the virtual array

Array interpolation technique explained in the previous section is applied and virtual circular arrays are formed by shifting the original array (see Figure 4.3). Each steering vector matrix is computed from Eq. (4.19) and possible interpolation errors are minimized by using least square estimation. The angular interval called in-sector (see Eq. 4.16) should be as small as possible to minimize the errors, but initially whole visibility area is defined as an in-sector interval, then the in-sector interval will be progressively reduced at each iteration.

- 2) Obtain spatially smoothed correlation matrix \bar{R}_{xx}
- 3) Perform MUSIC algorithm
- 4) Narrow down in-sector area

The angles whose power level is less than aP are removed from the in-sector where P is the maximum point in the MUSIC spectrum and “a” is a predetermined constant. Whole sequence might be repeated for a fixed number of iterations.

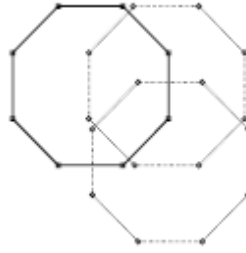


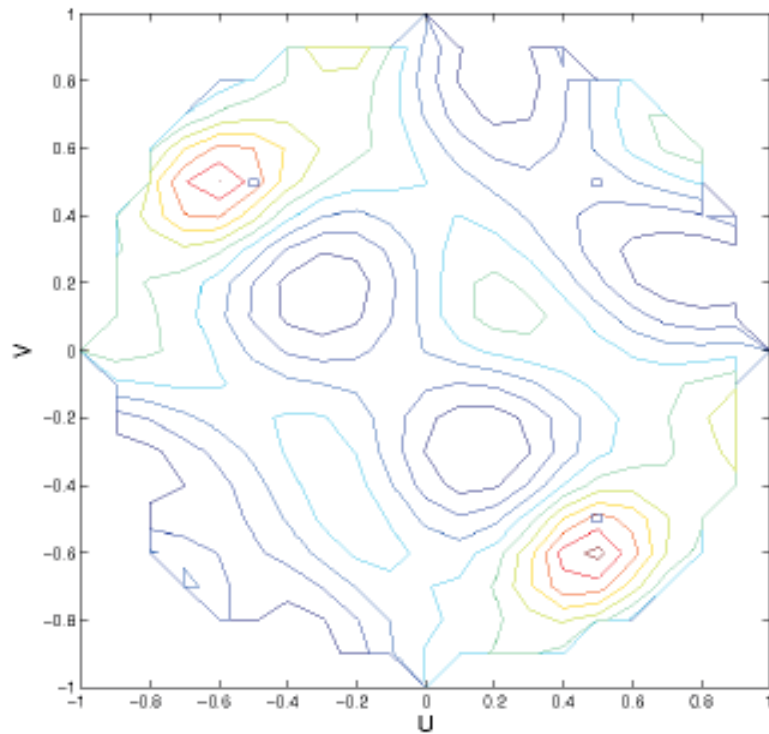
Figure 4.3: Array shifting example for planar arrays such as UCAs [22]

Simulated result of the iterative spatial smoothing algorithm can be seen in Figure 4.4. The signals source are fully correlated and coming from (45,45), (135,45), (-45,45) in azimuth and elevation, respectively. The array parameters are matched with the UCA of the direction finding system and simulated real array is shifted 9 times to generate virtual arrays. White Gaussian noise with 10dB SNR is added to the antenna output of the each array [22]. The blue squares on the power spectrum maps are the actual positions of the signals and the peaks of the contour plots refer to the estimated positions. MUSIC algorithm without spatial smoothing in Fig 4.4a shows that MUSIC localizes only approximate positions of the two correlated sources. MUSIC with suggested spatial smoothing method after 5 iterations works for all of the three correlated sources (see Figure 4.4b).

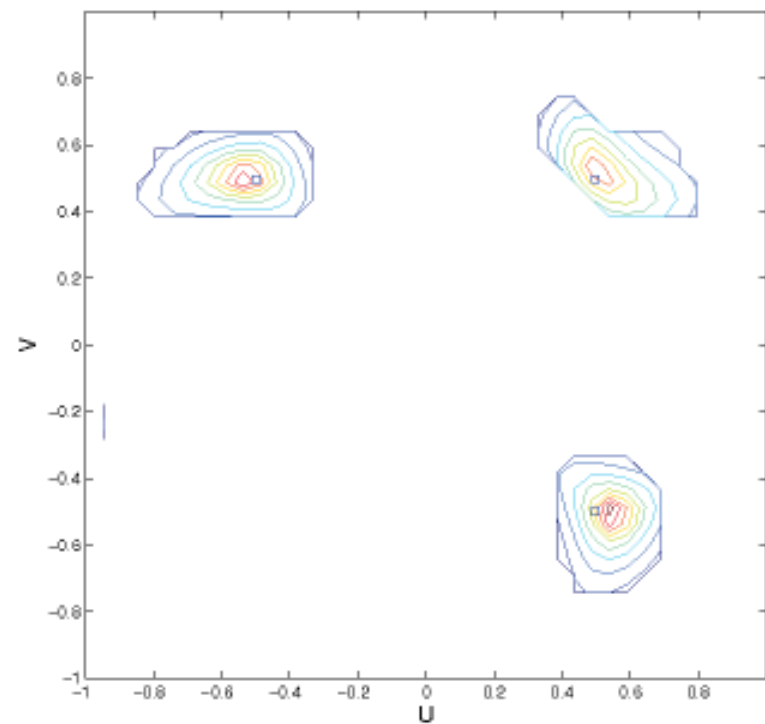
The suggested algorithm is applied to the 2D direction finding system with a passive RFID tag for an experiment. To generate coherent signals, a rectangular metallic plate is placed between the array and the tag. Metallic plate and the system can be seen in Figure 4.5.

The tag receives a query signal which is transmitted by the dipole antenna and prepares a response by using the power of the query. The response of the tag reaches the array from both 1) direct path and 2) reflection path.

The localization results of the tag with and without metal plate can be seen in Figure 4.6. Figure 4.6.a is the actual location of the tag and in Fig 4.6b, MUSIC algorithm doesn't include spatial smoothing pre-processing algorithm. It is clear that these results support the simulated results in Figure 4.4a. MUSIC algorithm finds the location of the point, where the tag signal hits the metal plate, by picking the largest point in the power spectrum since the signal coming from the reflection path is more intense than the direct path signal.



a)



b)

Figure 4.4: Results of the MUSIC algorithm for 3 correlated signals a) without spatial smoothing b) with spatial smoothing after 5 iterations [22]

The raw data obtained from multipath case is saved to use the same data with spatial smoothing algorithm. Unfortunately, suggested algorithm fails at localization of the correlated signals. The result of the MUSIC with spatial smoothing can be seen in Figure 4.7.

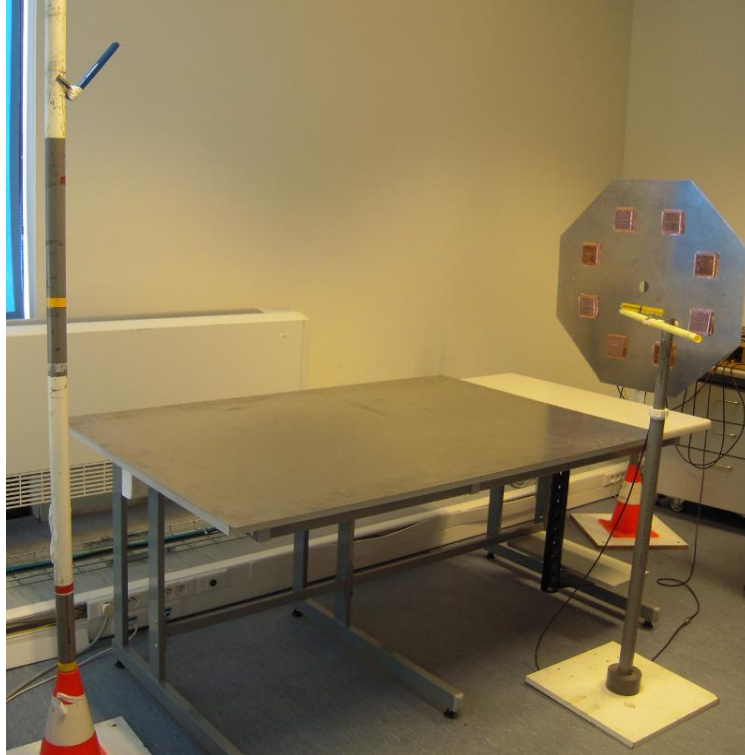
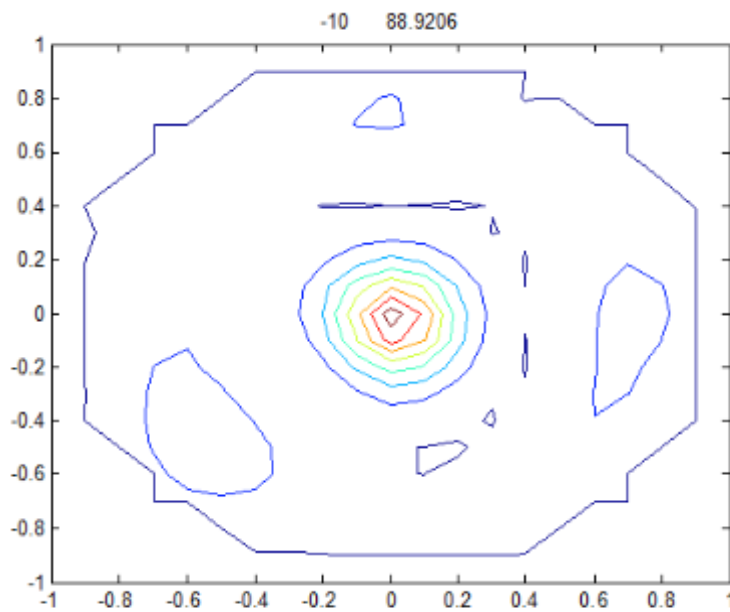
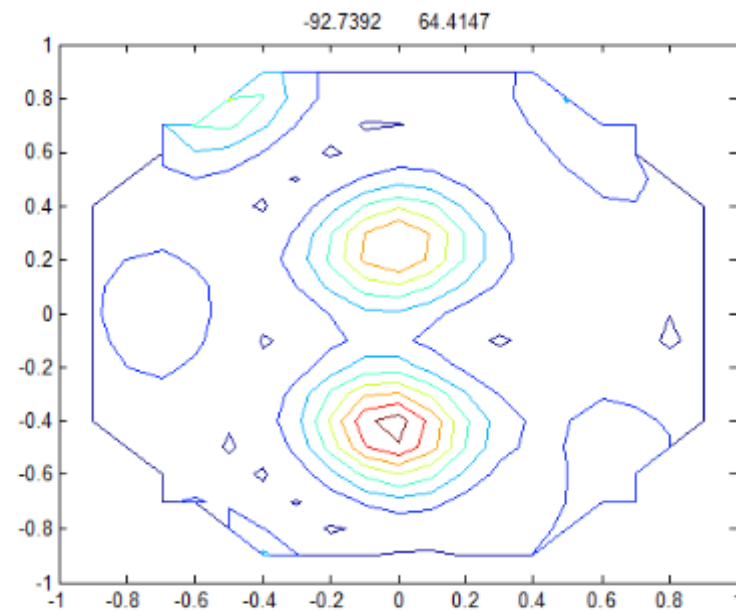


Figure 4.5: 2D direction finding system with coherent signals



a) real position of the tag (azimuth=-10, elevation=88.921)



b) estimated position of the tag in multipath environment (azimuth=-92.739, elevation=64.415)

Figure 4.6: Results of the MUSIC algorithm a) without metal plate b) with metal plate (correlated signals)

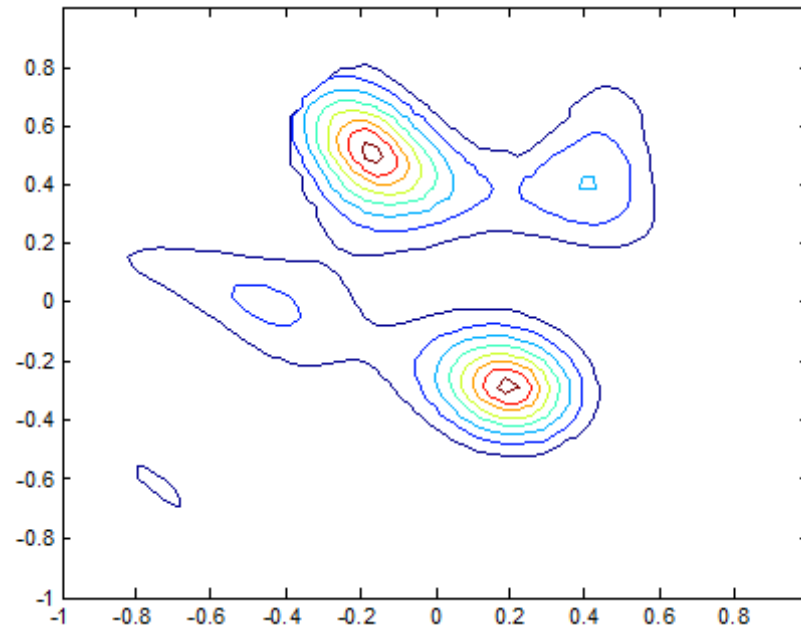


Figure 4.7: The result of the MUSIC algorithm with suggested spatial smoothing algorithm.

5. POST-PROCESSING APPROACH to MUSIC ALGORITHM for 2D DIRECTION FINDING SYSTEM: CLEAN ALGORITHM

A direction finding system for passive RFID tags is explained in Chapter 3 and a new spatial smoothing technique to avoid multipath effects and arrange the system for practical applications is introduced in Chapter 4. Besides these regulations, MUSIC algorithm might still fail in the presence of noise or when the sources are too close or when the source signal is too weak even though the signals are uncorrelated. In this chapter, it is suggested applying a post-processing method called Clean Algorithm to MUSIC algorithm. Suggested method is commonly used in interferometry imaging for radio astronomy.

A brief introduction to interferometry will be presented as background information. Then, mathematical relation of MUSIC algorithm and interferometric imaging, CLEAN algorithm, simulated and measured results of proposed approach will appear in the next sections.

5.1 Interferometry

Radio astronomic imaging is constructing sky map on the map by obtaining each pixels. The voltages received by the antennas are passed through voltage multiplier and integrator (see Figure 5.1). The output of the devices is called “visibility function” which relates to the aperture of the point source. The complex visibility function is [30-32]:

$$V(u, v) = \iint_S I(l, m) e^{-2\pi i(ul+vm)} dl dm \quad (5.1)$$

where (u, v) : is a coordinate system which is used to define the distances between any pair of antennas in terms of wavelength, S : denotes whole sky, $I(l, m)$: angular distribution of the source intensity, (l, m) : x and y components of a unit vector.

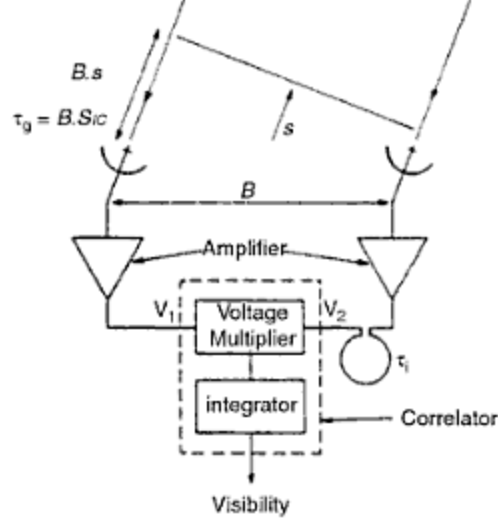


Figure 5.1: An interferometer with two antennas. B is the distance between antennas; V_1 and V_2 are antenna output voltages, τ_i is the instrumental delay and τ_g is geometric delay [31].

As seen in Eq. (5.1), the visibility function is Inverse Fourier Transform of the intensity function. Therefore, the intensity function can be obtained by applying Fourier Transform to visibility function. The intensity coming from a specific part of the sky is as follows [31]:

$$I(l, m) = \iint_S V(u, v) e^{2\pi i(ul+vm)} du dv \quad (5.2)$$

Eq. (5.2) is very time-consuming process; hence Fast Fourier Transform provides computational simplicity. However, the visibility function must be obtained on a regular grid to apply FFT. The gridded visibility function can be expressed as [30, 31]:

$$V_{grid}(u, v) = III(u, v) \{G(u, v) \otimes V_{meas}(u, v)\} = W(u, v) \{V_{meas}(u, v)\} \quad (5.3)$$

where $G(u, v)$: convolving function, \otimes : denotes convolution, $V_{meas}(u, v)$: measured visibility function on irregular grid, the Sha function:

$$III(u, v) = \sum_{r=-\infty}^{+\infty} \delta(u - u_r) \delta(v - v_r) \quad (5.4)$$

and the weighting function:

$$W(u, v) = \sum_{r=-\infty}^{+\infty} W_r \delta(u - u_r) \delta(v - v_r) \quad (5.5)$$

Uniform and Natural weighting are the widely used weighting functions. Natural weighting which accepts $W_r = 1$ provides best signal-to-noise ratio despite resulting in poor beam shape. Uniform weighting provides minimization of the sidelobes of the synthesized beam and accepts $W_r = 1/N_r(k)$ where $N_r(k)$ is the number of data points within the k th region [32]. Discrete Fourier Transform (DFT) can be applied the gridded visibility function in Eq. (5.3) to get intensity function. The intensity function is [30]:

$$I_D(l, m) = \sum_k W(u_k, v_k) \mathcal{V}_{meas}(u_k, v_k) e^{2\pi i(ul+vm)} dudv \quad (5.6)$$

The intensity function $I_D(l, m)$ is known as ‘‘Dirty Map’’. Measured visibility function has complex, normally distributed random error component $\mathcal{V}_{meas}(u, v) = V(u, v) + \xi(u, v)$. DFT of the measured visibility is the convolution of real intensity function and ‘‘Dirty Beam’’. Dirty Beam (DB) is the impulse response of the system to a point source (see Figure 5.2). Dirty Beam can be expressed as follows:

$$B_D(l, m) = \sum_k W(u_k, v_k) e^{2\pi i(ul+vm)} dudv \quad (5.7)$$

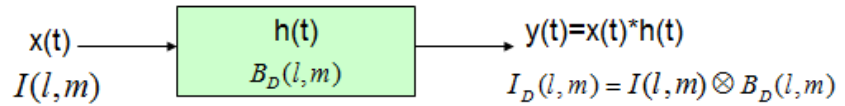


Figure 5.2: Schematic demonstration of intensity and dirty beam

To obtain real intensity, a deconvolution method such as CLEAN or Maximum Entropy Deconvolution Method (MEM) can be applied to dirty map.

5.2 Mathematical Link between Interferometry and MUSIC Algorithm

As mentioned in Chapter 3, an alternative version of MUSIC power equation is used by the direction finding system. Remember Eq. (3.1):

$$P(\bar{k}) = \frac{1}{\bar{e}(\bar{k})^H \bar{U}_N \bar{U}_N^H \bar{e}(\bar{k})} \quad (5.8)$$

where $\bar{e}(\bar{k})$: a column vector of phase delay of the antenna array and i th element is :

$$e_i = e^{i\bar{k}\bar{r}_i} \quad (5.9)$$

where \bar{k} : propagation vector, \bar{r}_i : the position of i th antenna

By using following relation of the signal and noise subspaces of the correlation matrix and inverting Eq. (5.8) [22],

$$I = U_S U_S^H + U_N U_N^H \quad (5.10)$$

DOA might be estimated by finding the minimum in the power spectrum. Inverted power is [22]:

$$P^{-1}(\bar{k}) = \bar{e}(\bar{k})^H I \bar{e}(\bar{k}) - \bar{e}(\bar{k})^H U_S U_S^H \bar{e}(\bar{k}) \quad (5.11)$$

The first part of Eq. (5.11) is equal to a constant N which is the number of antenna in this case. If this constant is ignored and the negative sign is removed, a MUSIC variant is obtained and DOA can be estimated by finding the maximum in the new power spectrum the MUSIC variant power is [22]:

$$\begin{aligned} P'(\bar{k}) &= \bar{e}(\bar{k})^H U_S U_S^H \bar{e}(\bar{k}) \\ &= \sum_{i_1} \sum_{i_2} a_{i_1 i_2} e_{i_1} e_{i_2}^* \end{aligned} \quad (5.12)$$

where $U_S U_S^H$ can be defined as the filtered version of the correlation matrix R_{xx} with elements a_{i_1} and a_{i_2} , i_1 : rows of filtered correlation matrix and i_2 : columns of filtered correlation matrix.

The power spectrum of the alternative and original MUSIC definitions give exactly the same source directions and for this reason the result of the original distribution have not been plotted in this chapter.

Hislop and Craeye suggested calling the visibility function in interferometric imaging as correlation matrix. Next step is showing the similarity of MUSIC variant and dirty map.

The propagation vector in terms of (l,m) and antenna positions in terms of (u,v) are respectively [22]:

$$\bar{k} = \frac{2\pi}{\lambda} (l\hat{x} + m\hat{y} + \sqrt{1-l^2-m^2}\hat{z}) \quad (5.13)$$

$$\bar{r}_i - \bar{r}_{i_2} = \lambda(u\hat{x} + v\hat{y} + 0\hat{z}) \quad (5.14)$$

By using Eq. (5.13) and (5.14) to rewrite Eq. (5.6),

$$I_D(l, m) = \sum_{i_1} \sum_{i_2} b_{i_1 i_2} e_{i_1} e_{i_2}^* \quad (5.15)$$

where $b_{i_1 i_2}$: elements of correlation matrix (visibility function)

Note that the weight function is assumed to be natural for simplicity. It is clear that there is a direct mathematical relation between Eq. (5.12) which represents MUSIC power spectrum and Eq. (5.15) which represents the dirty map. Therefore, a post-processing algorithm such as CLEAN to avoid sidelobe effects can be applied to the MUSIC variant.

5.3 The CLEAN Algorithm

Clean algorithm was proposed by Högbom in 1978 to reconstruct Clean Map from Dirty Map in order to reduce sidelobe effects [34, 35]. Clark and Cotton-Schwab algorithms are the variant of Högbom's CLEAN algorithm. The basic assumption of CLEAN and CLEAN variant algorithms is that the presence of noise and sidelobes don't make significant difference on magnitude and position of the point source [35].

CLEAN algorithm is an iterative post-processing method and defines two new concepts: Clean Map (CM) and Clean Beam (CB) besides Dirty Map and Dirty Beam. Clean Map is used for constructing the noise free map at each step of this algorithm and it is initialized with zero. It has been shown that Dirty Map, in other words intensity, is DFT of visibility function. Clean Beam is an ideal impulse response which consists of only one main lobe, usually Gaussian, where DB is the real impulse response of the system to a point source. The components of Dirty Beam are a main lobe and several sidelobes.

The steps of the CLEAN algorithm are as follows [32-35]:

1) Compute the Dirty Map and Dirty Beam

For direction finding system, the first of this step is computing the power spectrum because as mathematically proven in the previous section, Dirty Map context in radio astronomy corresponds to power spectrum context in direction finding. If there is only one point source in the environment, the signal received

by the direction finding system will be Dirty Beam which is the impulse response of the system. The signal received by the data collector is a convolution of the original signal and impulse response. The power spectrum is:

$$I_D(l, m) = P(\bar{k}) = \sum_{i_1} \sum_{i_2} a_{i_1 i_2} e_{i_1} e_{i_2}^* \quad (5.16)$$

By considering the relation of DM and DB in Eq. (5.6) and (5.7) and corresponding context in direction finding, DB can be expressed as follows for direction finding system.

$$B_D(l, m) = \sum_{i_1} \sum_{i_2} e_{i_1} e_{i_2}^* \quad (5.17)$$

- 2) Find the maximum absolute value on the map $|I_0|$. Shift the DB to that point and normalize DB to $\gamma|I_0|$ at the beam centre. Subtract normalized and shifted DB from DM to get the residual. γ is a damping factor and called loop gain ($0 < \gamma \leq 1$).
- 3) Shift the Clean Beam to the position of the maximum, normalize it to $\gamma|I_0|$ at the beam centre and add it to the residual map.
- 4) Return to step 2 until there is no significant intensity left on the Dirty Map.
- 5) Add the last residuals to Clean Map which is formed at step 4 (this step is optional). If the residuals aren't added, the Clean Map will be cleaner (see Figure 5.4).

The main purpose of this method is finding each significant peak in the power spectrum and removing side lobes for each peak which most probably signs the DOA of the source by swapping the Dirty Beam with Clean Beam.

5.4 Simulated Results

For simulations, UCA with eight sensors is assumed to have 0.3m radius. "ns" (number of sources) and the positions of the sources have to be known. Identically distributed white Gaussian noise might be added optionally while generating ns uncorrelated signals. The blue crosses, circles and squares represent the real source positions and the green stars, crosses and squares are the estimated positions of the point sources for all simulated and measured results.

In Figure 5.3, there are two uncorrelated signals located at Cartesian coordinates $(x,y,z) = [-10, 0,100]$ and $[10, 0,100]$ (metres) with an operating frequency of 868MHz in the absence of noise (Figure 5.3a) and in the presence of noise (Figure 5.3b, 5.3c). For these two close sources, MUSIC variant finds the locations of the sources correctly in noise free space. However, when independent identically distributed white Gaussian noise was added at each antenna output with SNR=0dB, MUSIC variant fails. After adding Gaussian noise, the weakest signal Eigen-value dropped to below the strongest of the noise Eigen-values leading to an incorrect representation of the signal subspace. Therefore MUSIC finds one of the sources and locates the other one in the valley of spectrum. CLEAN algorithm fixes sidelobe effect problem and after three iterations, the exact locations of both of the sources were found. The last step of the CLEAN algorithm, adding the residuals to Clean Map is applied in this example. If not, the iteration number had to be increased to twelve to choose two significant peaks in the power spectrum (see Figure 5.4).

As seen in Figure 5.4, the final map of the power spectrum by ignoring the fifth step is cleaner despite more iteration requirement.

In Figure 5.5, there are two uncorrelated signals located very close to each other ($(x,y,z) = [-7,0,100]$ and $[7,0,100]$ (metres)) with same operating frequency. Because of the sources being too close, the significant peaks in the power spectrum formed together as one peak and there was only one significant peak in the spectrum, thus MUSIC algorithm fails even in noise free space. On the other hand, CLEAN algorithm separated these two peaks after 3 iterations both noisy and noise free space. The results of the MUSIC and CLEAN can be seen in Figure 5.5.

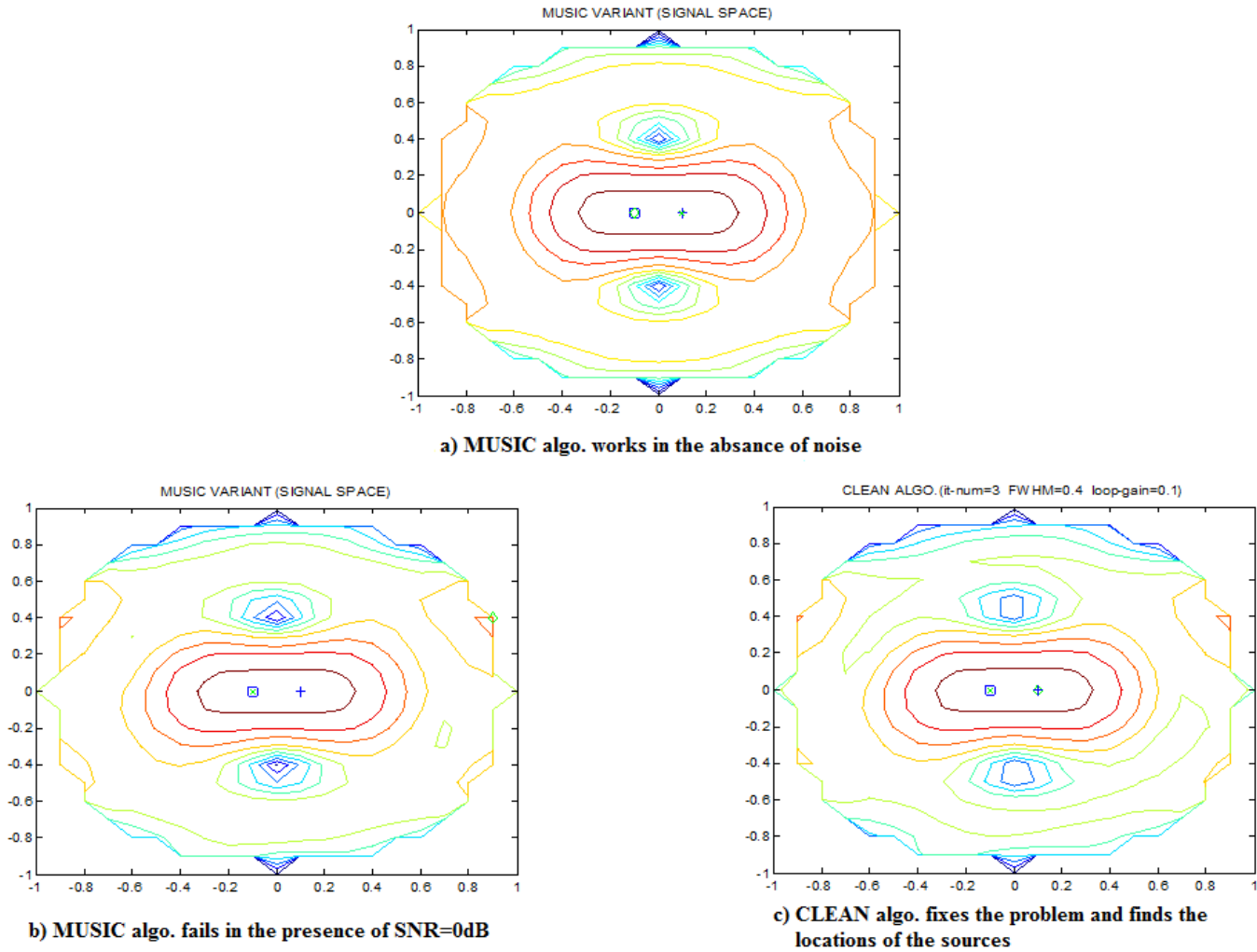


Figure 5.3: Two uncorrelated sources located at $(x,y,z) = [-10,0,100]$ and $[10,0,100]$ (metres) **a)** MUSIC algo. result in the absence of noise **b)** MUSIC algo. result in the presence of noise (SNR=0dB) **c)** CLEAN algo. result after three iterations in the presence of noise (SNR=0dB)

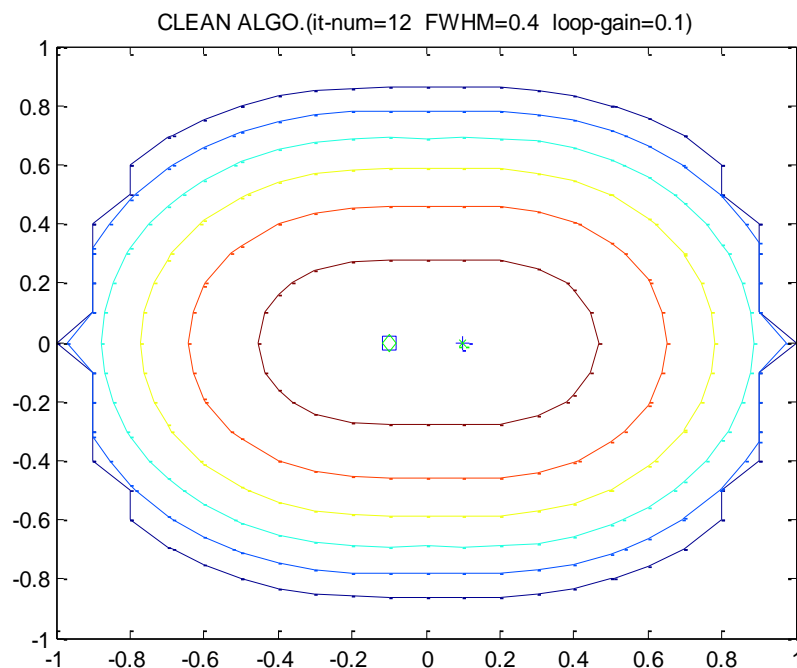


Figure 5.4: The final map of the power spectrum without adding residuals

Another example is that three uncorrelated signals coming from Cartesian coordinates $(x,y,z) = [-40,0,100]$, $[40,0,100]$ and $[1,0,100]$ (metres). MUSIC worked for three point sources at these locations when there was no noise and failed when $\text{SNR}=-10\text{dB}$ (see Figure 5.6). The reason of the failure of MUSIC in Figure 5.6b is similar to failure in Figure 5.3b: replacement of signal and noise-subspaces.

In the next example, the locations of the sources are $(x,y,z) = [-20,40,100]$, $[20,40,100]$ and $[1,0,100]$ (metres). MUSIC algorithm fails in both noisy and noise free space because of the sidelobe effects and CLEAN works in both (see Figure 5.7).

As seen in the simulated results that CLEAN post-processing algorithm fixes sidelobes effects, peak overlapping in the power spectrum and signal and noise subspace replacement. The main reason for MUSIC's failure is that it doesn't take into account the impulse response of the array to a point source as does CLEAN.

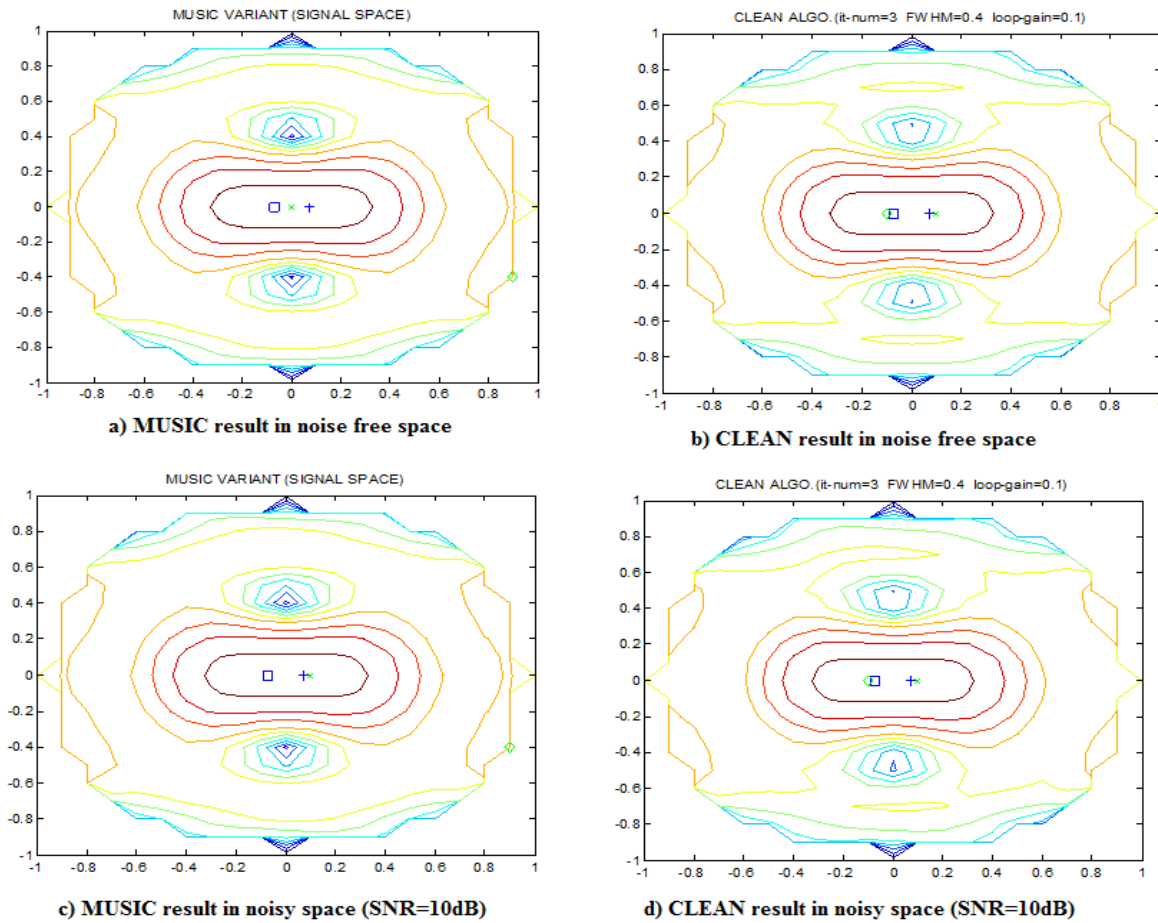


Figure 5.5: Two uncorrelated sources located at $(x,y,z) = [-7,0,100]$ and $[7,0,100]$ **a)** MUSIC algo. result in noise free space **b)** CLEAN algo result in noise free space **c)** MUSIC algo. result in noisy space(SNR=10dB) **d)** CLEAN algo. result after three iterations in noisy space(SNR=10dB).

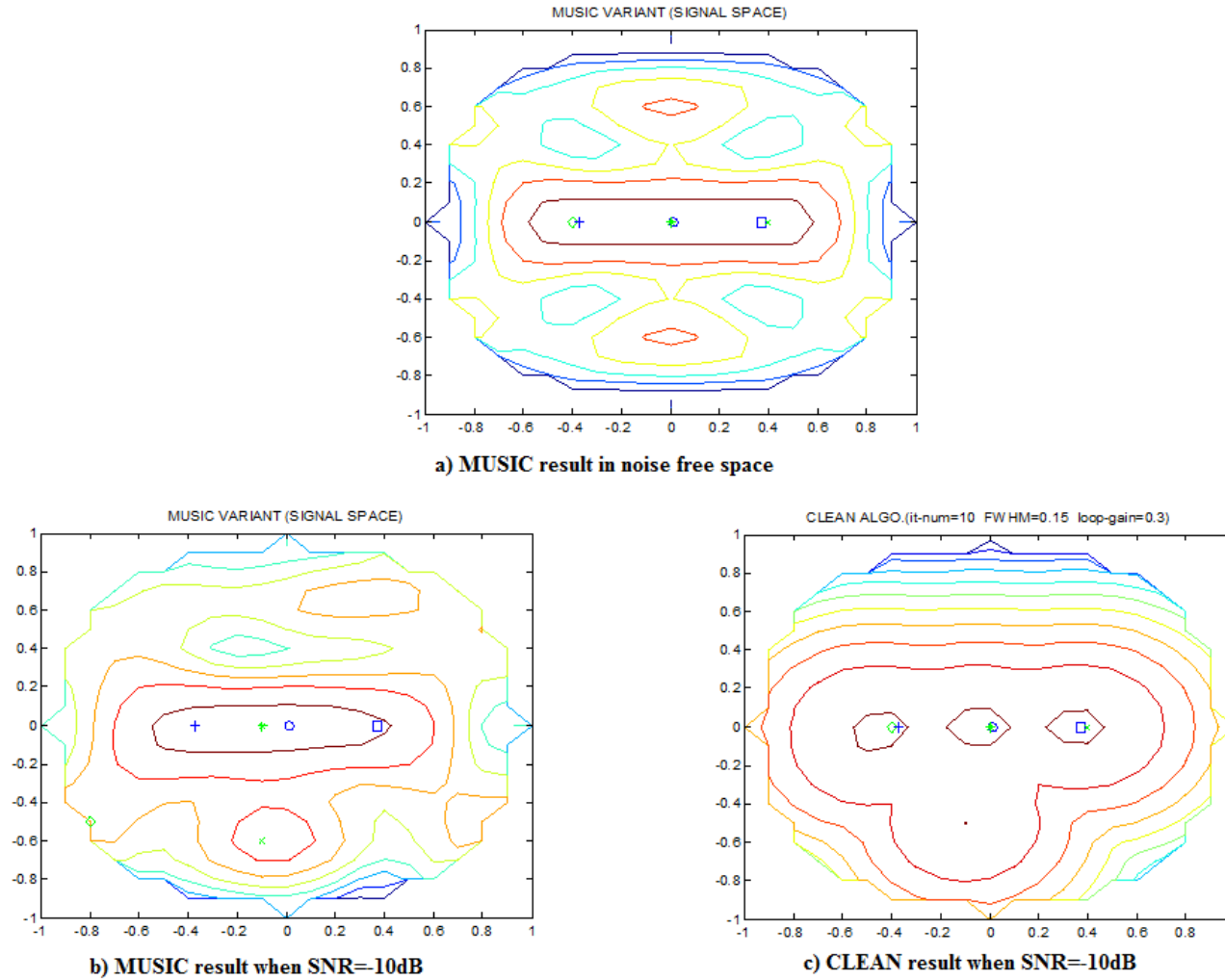


Figure 5.6: Three uncorrelated sources located at $(x,y,z) = [-40,0,100]$, $[40,0,100]$ and $[1,0,100]$ **a)** MUSIC algo. result in the absence of noise **b)** MUSIC algo. result in noisy space (SNR=-10dB) **c)** CLEAN algo. result after ten iterations in noisy space (SNR=-10dB)

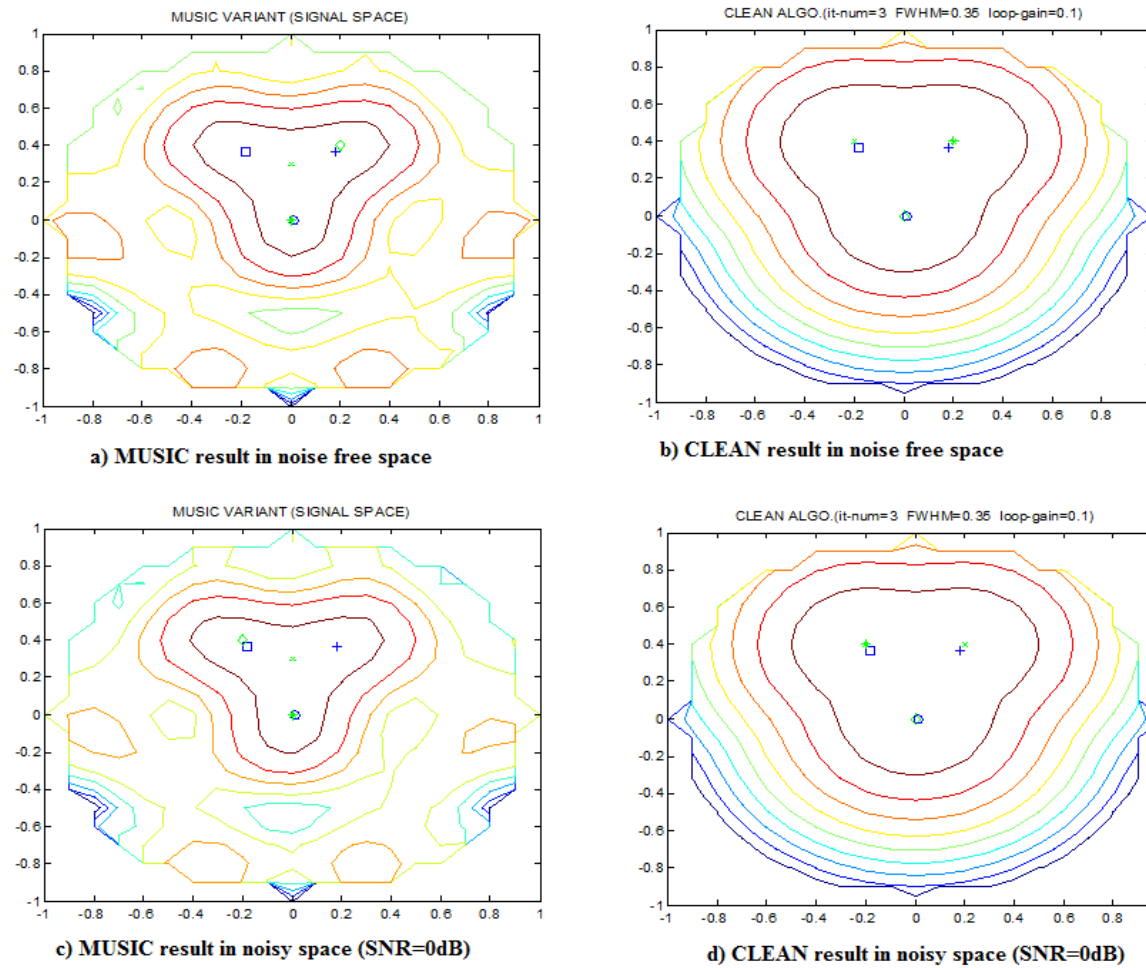


Figure 5.7: Two uncorrelated sources located at $(x,y,z) == [-20,40,100]$, $[20,40,100]$ and $[1,0,100]$ **a)** MUSIC algo. result in noise free space **b)** CLEAN algo result in noise free space **c)** MUSIC algo. result in noisy space(SNR=10dB) **d)** CLEAN algo. result after three iterations in noisy space(SNR=10dB).

5.5 Measured Results

The direction finding system for passive RFID tags is explained in Chapter 3 in detail and this system can localize only one source because the reader can communicate with one tag at each time. To prove CLEAN algorithm works with direction finding system besides simulations, dipole antenna is fed by oscillator with desired amplitude to obtain fake tag and the reader was removed from the system. Locating the dipoles vertically was preferred to minimize mutual coupling effect between antennas.

Figure 5.8a and 5.8b are the power spectrums of two vertical sources after MUSIC and CLEAN, respectively. The upper one is located at $(u,v)=[0.3607\ 0.3549]$ and -15dBm; the lower one is located at $[0.4021\ 0.0190]$ and its amplitude is -30dBm. The amplitudes and positions of the sources in Figure 5.8c and 5.8d are amplitudes=-15dBm and $(u,v)=[0.3607\ 0.3549]$ and $[0.3993\ 0.0613]$.

For three sources case, three dipole antennas were connected to the oscillators and the generated signals were that signal showed with blue square had -15dBm amplitude and coming from $(u,v)=[-0.4322\ 0.3838]$; blue cross' amplitude and location were -15dBm and $(u,v)=[0.6068\ 0.5225]$ respectively. The blue circle represented the signal coming from $(u,v)=[6.3093e-004\ 6.5960e-005]$ and had -5dBm amplitude level. DOA estimation results after MUSIC and CLEAN algorithms can be seen in Figure 5.9.

The effectiveness of post-processing deconvolution algorithm is just proved with both simulated and measured results. In Figure 5.8, MUSIC can only find one of the signal sources, but CLEAN finds both. Similarly, CLEAN finds all three sources in Figure 5.9, but MUSIC finds only two. Measured results indicate that CLEAN algorithm fixes the encountered problems in practical applications.

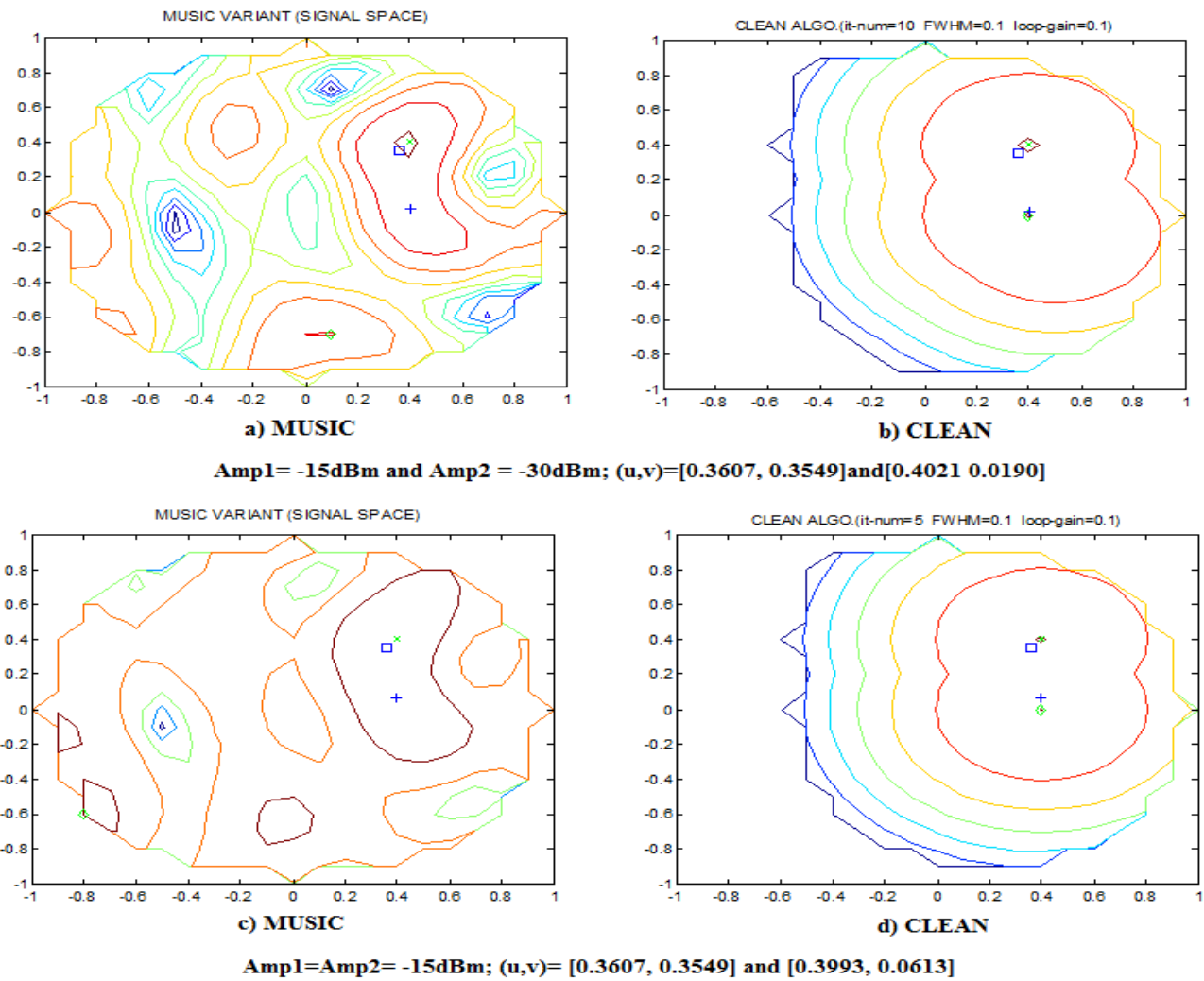


Figure 5.8: The measured results of MUSIC and CLEAN algorithms for two different amplitude and position conditions

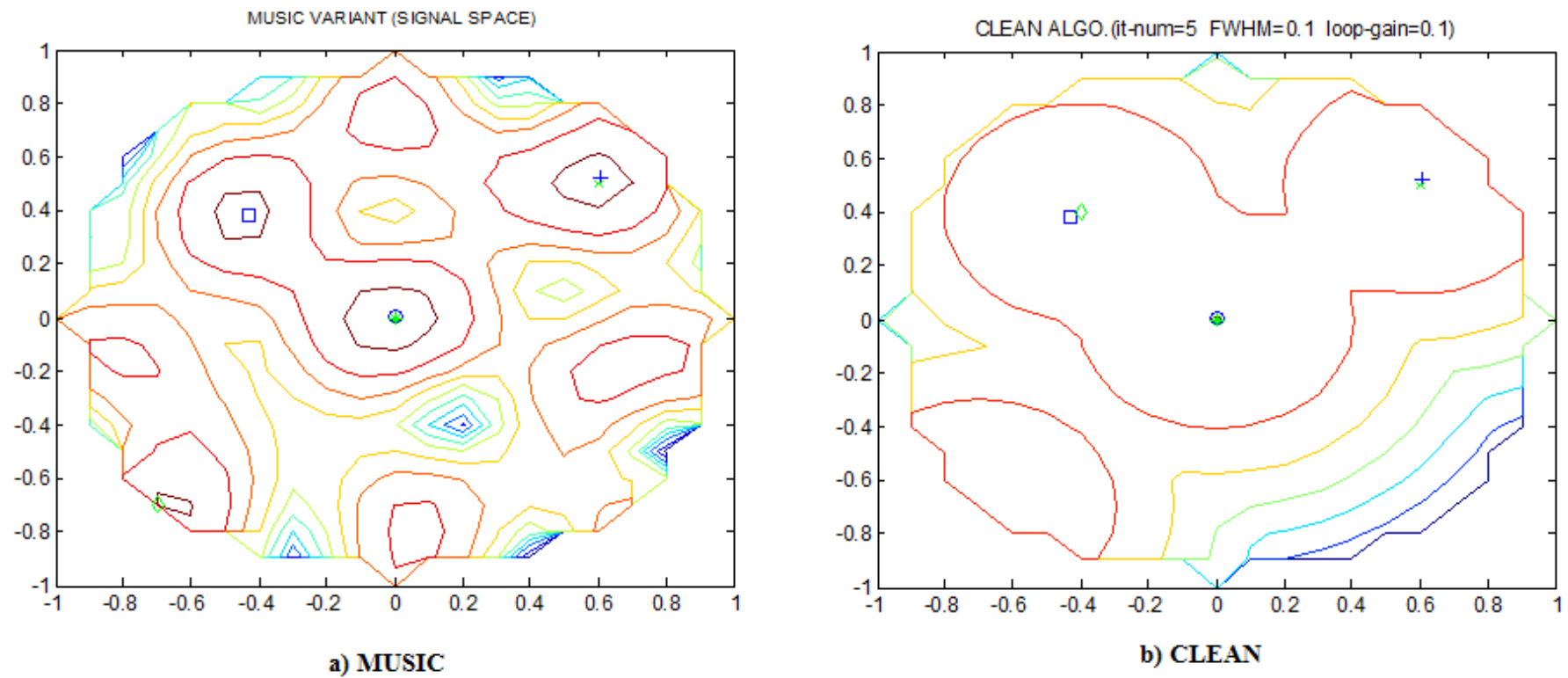


Figure 5.9: The measured results of MUSIC and CLEAN algorithms for three sources located at $(u,v) = [-0.4322 \ 0.3838]$, $[0.6068 \ 0.5225]$ and $[6.3093e-004 \ 6.5960e-005]$ and the corresponding amplitudes are -15dBm, -15dBm and -5dBm.

6. CONCLUSION

In this thesis, DOA estimation literature is summarized, 2-D direction finding system is introduced, cheap and easy array recalibration technique is suggested for this system, measured results of spatial smoothing pre-processing application on this system is presented and finally applying a post-processing algorithm on this system to discard sidelobe effects is proposed. The main purpose of this work is calibrating the system out of the laboratory and improving the accuracy of localization process.

Array calibration is very important process to estimate the direction of the source for direction finding systems. The used 2D direction finding system should be calibrated in the field easily and accurately in the case of it become a commercial product. Instead of using a self calibration technique which is a time-consuming process, a recalibration technique is proposed to calibrate the system the system out of the laboratory. The new technique is used the first row of the correlation matrix of the tag in the first state and the first row of the correlation matrix of the dipole both in the first state and in the second state to calculate the calibration vector for the second state. If the localization results of the recalibrated system (see Figure 3.13) are compared with the localization results of the calibrated system (with calibration tag, see 3.7), it can be easily said that the proposed method works successfully although the direction estimates of the recalibrated system have slight sidelobe effects. These effects are expected because the raw data of the dipole antenna is also used to recalibrate the system besides the raw data of the tag.

The DOA estimation algorithm of the used system is MUSIC. The major drawback of this algorithm is that it doesn't work in the presence of correlated signals. Anechoic environment experiments of a new spatial smoothing algorithm which is proposed by the designers of the 2D direction finding system are made and the results of the experiment are presented in the forth chapter. The algorithm provides to overcome the multipath effect problems for used direction finding system. It is seen in measured results that the suggested pre-processing algorithm doesn't solve the multipath effect problems although it works reliably on simulated data.

The problem with the measured results is that the antenna patterns are not correctly accounted for. More precisely the patterns are different for each antenna due to their differing positions relative to the edge of the ground plane and due to mutual coupling. This should cause problems with the interpolation of the array. As mentioned before, the array calibration technique discards the phase-amplitude mismatch effects of the sensors and cable mismatch effects, but not mutual coupling effect. Actually, the mutual coupling effect isn't a big deal in the absence of multipath. In multipath environment, mutual coupling effect increases the array interpolation errors while generating virtual antenna arrays. The phase response of the antennas may not be the same for all the antennas and will probably vary more significantly at small elevations than large ones. As reflections are typically at smaller elevations, they are more susceptible for this problem. Measure the antenna patterns and including them in the steering vectors of the MUSIC implementation or simulating the steering vectors might be the possible solutions for this problem.

MUSIC algorithm does not into account the non-ideal impulse response of typical direction finding arrays. In the fifth chapter, applying a post-processing approach to MUSIC algorithm is suggested to improve the localization accuracy of direction finding system. Suggested post-processing method- CLEAN is commonly used in interferometric imaging to account for the effects of the non-ideal impulse response on images of the celestial sphere. On the basis of the mathematical link between MUSIC and interferometry, applying the CLEAN algorithm rectifies this problem. According to the simulated and measured results in chapter five, MUSIC and CLEAN combination provides better results than MUSIC for two important cases: closely spaced sources and weak sources. The CLEAN algorithm swaps each significant peak -Dirty Beam in MUSIC power spectrum with ideal impulse response -Clean Beam. For this reason, proposed provides noise filtering and better resolution.

REFERENCES

- [1] **Foutz J., Spanias A. and Banavar M. K.**, 2008: *Narrowband Direction of Arrival Estimation for Antenna Arrays*, 1st ed., Morgan & Claypool Publishers.
- [2] **Khan Z. I., Kamal M. MD, Hamzah N., Othman K. and Khan N. I.**, 2008. Analysis of Performance for Multiple Signal Classification (MUSIC) in Estimating Direction of Arrival. *IEEE International RF and Microwave Conference Proceedings*, Kuala Lumpur, Malaysia, December 2-4.
- [3] **Chen Z., Gokeda G. and Yu Y.**, 2010: *Introduction to Direction-of-Arrival Estimation*, Artech House.
- [4] **Weber Z. and Huang Y.**, 2009: Analysis for Capon and MUSIC DOA Estimation Algorithms, *Antennas and Propagation Society International Symposium. IEEE*, Charlston SC, U.S., June 1-5.
- [5] **Bo W.**, 2006. Realization and Simulation of DOA estimation using MUSIC Algorithm with Uniform Circular Arrays, *The 4th Asia-Pasific Conference on Envirenmental Electromagnetics CEEM 2006*, Dalian , August 1-4.
- [6] **De Leon F. A. and Marciano J. J. S.**, 2006. Application of MUSIC, ESPRIT and SAGE Algorithms for Narrowband Signal Detection and Localization, *IEEE Region 10 Conferance TENCON*, Hong Kong , November 14-17.
- [7] **Schmidt R. O.**, 1986: Multiple Emitter Location and Signal Parameter Estimation *IEEE Trans on Antennas and Propagation*, Vol. **34**, pp. 276-280.
- [8] **Gershman A. B., RübSamen M. and Pesavento M.** 2010: One- and two-dimensional direction-of-arrival estimation: An overview of search-free techniques, *Signal Processing*, Vol. **90**, pp. 1338-1349.
- [9] **Wei Z. and Xiaoli X.**, 2007: Analysis and Simulation of the Direction of Arrival Estimation Algorithm of Spatial Signal. *The Eight International Conferance on Electronic Measurement and Insturements.*, Xi'an, China, August 6-18.
- [10] **Roy R. and Kailath T.**, 1989: ESPRIT-Estimation of Signal Parameters Via Rotational Invariance Techniques, *IEEE Trans on Acoustics, Speech and Signal Processing*, Vol. **37**, pp. 984-995.
- [11] **Gao F. and Gershman A. B.**, 2005: A Generalized ESPRIT Approach to Direction-of-Arrival Estimation, *IEEE Signal Processing Letters*, Vol. **12**, pp. 254-257.

- [12] **Paulraj A., Roy R. and Kailath T.**, 1985: Estimation of Signal Parameters Via Rotational Invariance Techniques-ESPIRIT, *Circuits, Systems and Computers. Nineteenth Asilomar Conference*, November 6-8.
- [13] **Stoica P. and Sharman K. C.**, 1990: Maximum Likelihood Methods for Direction-of-Arrival Estimation, *IEEE Trans on Acoustics, Speech and Signal Processing*, Vol. **38**, pp. 1132-1143.
- [14] **Hislop G., Drouget M. and Craeye C.**, 2010. Aprototype 2D Direction Finding System with Passive RFID Tags. *Proceedings of the Fourth European Conference on Antennas and Propagation (EuCAP)*, Barcelona, Spain, April 12-16.
- [15] **Aberbour L., Craeye C. and Decostre A.**, 2008. Low Profile Compact-Slot Antenna Array for RFID Applications: Backscatter-Tag Identification and Localization. *AP-S IEEE Trans Antennas and Propagation Society International Symposium*, San Diego, CA, USA, July 5-11.
- [16] <http://www.epcglobalinc.org/standards/uhfclg2/uhfclg2_1_0_9-standard-20050126.pdf>, accessed at 25.10.2010.
- [17] **Hislop G. and Craeye C.**, "On the Mathematical Link between the MUSIC Algorithm and Interferometric Imaging", *Accepted for and awaiting publication in the IEEE Transactions on Antennas and Propagation*.
- [18] **Reed J. H.**, 2002: Software Radio: A Modern Approach to Radio Engineering Prentice Hall PTR, New Jersey, USA.
- [19] **Dandekar K. R., Ling H., and Xu G.**, 2000. Smart Antenna Array Calibration Procedure Including Amplitude and Phase Mismatch and Mutual Coupling Effects. *IEEE International Conference on Personal Wireless Communications*, Hyderabad, India, December 17-20.
- [20] **Zeng Z. and Ma H.**, 2009: Subspace-Based Self-calibration of Mutual Coupling in Uniform and Circular Array. CISP 2nd International Congress on Image and Signal Processing, Tianjin, China, October 17-19.
- [21] **Evans J. E. and Sun F.**, 1981: High resolution angular spectrum estimation techniques for terrain scattering analysis and angle of arrival estimation. *1st ASSP Workshop on Spectral Estimation*, Hamilton, Ont., Canada.
- [22] **Hislop G. and Craeye C.**, 2009: Spatial smoothing for 2D direction finding with passive RFID tags. *LAPC Antennas and Propagation Conference*, Loughborough, UK, November 16-17.
- [23] **Shan T., Wax M. and Kailath T.**, 1985: On spatial smoothing for direction of arrival estimation of coherent signals. *IEEE Transactions on Acoustics, Speech and Signal Processing*, Vol. **33**, pp. 806-811.
- [24] **Wang H. and Lui K.**, 1998: 2D spatial smoothing for multipath coherent signal separation. *IEEE Transactions on Aerospace and Electronic Systems*, Vol. **34**, pp. 391-405.

- [25] **Friendlander B. and Weiss A. J.**, 1992: Direction Finding Using Spatial Smoothing With Interpolated Arrays. *IEEE Transactions on Aerospace and Electronic Systems*, Vol. **28**, pp. 574-586.
- [26] **Pillai S. U. and Kwon B. H.**, 1989: Forward/Backward Spatial Smoothing Techniques for Coherent Signal Identification. *IEEE Transactions on Acoustics, Speech and Signal Processing*, Vol. **37**, pp. 8-14.
- [27] **Tompson J. S., Grant P. M. and Mulgey B.**, 1996: Performance of Spatial Smoothing Algorithms for Correlated Sources. *IEEE Transactions on Signal Processing*, Vol. **44**, pp. 1040-1045.
- [28] **Lau B. K., Cook G. J. and Leung Y. H.**, 2004: An Improved Array Interpolation Approach to DOA Estimation in Correlated Signal Environment. *IEEE International Conference on Acoustics, Speech and Signal Processin* , May 17-21.
- [29] **Pesavento M., Gershman A. B. and Luo Z.**, 2002: Robust Array Interpolation Using Second-Order Cone Programming. *IEEE Signal Processing Letters*, Vol. **9**, pp. 8-11.
- [30] **Cornwell T. and Braun R.**, 1989: "Deconvolution" in Synthesis Imaging in Radio Astronomy, *Astronomical Society of the Pacific Conference Series*, Vol. **6**, pp. 167-183.
- [31] **Rohlfs K. and Wilson T. L.**, 2004: *Tools of Radio Astronomy*, 4th ed., Springer, Hamburg, Germany, pp. 203-218.
- [32] **Thompson A. R., Moran J. M. and Swenson G. W.**, 2004: *Interferometry and Synthesis in Radio Astronomy*, 2nd ed., Wiley.
- [33] **Högbom J. A.**, 1974: Aperture Synthesis with a Non-Regular Distribution of Interferometer Baselines. *Astronomy and Astrophysics Supplement*, Vol. **15**, pp. 417-426.
- [34] **Tsao J. and Steinberg B. D.**, 1988: Reduction of Sidelobe and Speckle Artifacts in Microwave Imaging: The CLEAN Technique. *IEEE Transactions on Antennas and Propagation*, Vol. **4**, pp. 543-556.
- [35] **Akhdar O., Mouhammadou M., Carsenat D., Decroze C. and Monediere T.**, 2009: A New CLEAN Algorithm for Angle of Arrival Denoising. *IEEE Antennas and Wireless Propagation Letters*, Vol. **8**, pp. 478-481.

APPENDICES

APPENDIX A.1 : MATLAB Computer Programme

CURRICULUM VITAE



Candidate's full name: Nida SAKAR

Place and date of birth: MERSİN / 23.12.1984

**Permanent Address: Soğanlı mah. Umut cad. Kevser Apt No: 11/13
Bahçelievler İSTANBUL**

Universities: İTÜ